Title: Brain-released alarmins and stress response synergize in accelerating atherosclerosis progression after stroke.

Authors: Stefan Roth[1,2], Vikramjeet Singh[1,2], Steffen Tiedt[1,2], Lisa Schindler[1,2], Georg Huber[3], Arie Geerlof[3], Daniel J Antoine[4], Antoine Anfray[5], Cyrille Orset[5], Maxime Gauberti[5], Antoine Fournier[5], Lesca M Holdt[6], Helena Erlandsson Harris[7], Britta Engelhardt[8], Marco E. Bianchi[9], Denis Vivien[5], Christof Haffner[1], Jürgen Bernhagen[1,2], Martin Dichgans[1,2], Arthur Liesz[1,2]*

Affiliations:

[1] Institute for Stroke and Dementia Research, Klinikum der Universität München, 81377 Munich, Germany

[2] Munich Cluster for System Neurology (SyNergy), 80336 Munich, Germany

[3] Institute of Structural Biology, Helmholtz Centre Munich, 85764 Munich, Germany

[4] MRC Center for Drug Safety Science, Department for Molecular and Clinical Pharmacology, University of Liverpool, L69 3GE, UK

[5] Inserm, Université de Caen-Normandie, CHU de Caen, Inserm UMR-S U1237, Physiopathology and Imaging of Neurological disorders (PhIND), - GIP Cyceron, 14074 Caen, France

[6] Institute of Laboratory Medicine, Klinikum der Universität München, 81377 Munich, Germany

[7] Department of Medicine, Karolinska University Hospital, SE-171 76 Stockholm, Sweden

[8] Theodor Kocher Institute, University of Bern, Freiestrasse 1, 3012 Bern, Switzerland.

[9] Faculty of Medicine, San Raffaele University, 20132, Milan, Italy

*To whom correspondence should be addressed: Arthur Liesz, M.D., Institute for Stroke and Dementia Research, 81377 Munich, Germany, E-Mail: Arthur.Liesz@med.uni-muenchen.de

One Sentence Summary: We demonstrate exacerbation of atherosclerosis after stroke and identified synergy of a catecholaminergic stress-response and alarmin-dependent signaling as a therapeutic target for recurrent vascular events.

Abstract: Stroke induces a multiphasic systemic immune response but the consequences of this response on atherosclerosis—a major source of recurrent vascular events—are barely investigated. Here we show that stroke exacerbates atheroprogression via alarmin-mediated propagation of vascular inflammation. The prototypic brain-released alarmin High mobility group box 1 protein (HMGB1) induced monocyte and endothelial activation via the receptor for advanced glycation end products (RAGE)-signaling cascade, and increased plaque load and vulnerability. Recruitment of activated monocytes via the CC-chemokine ligand 2 – CC-chemokine receptor type 2 (CCL2-CCR2) pathway was critical in stroke-induced vascular inflammation. Neutralization of circulating alarmins or knockdown of RAGE attenuated atheroprogression. Blockage of β3-adrenoreceptors attenuated the egress of myeloid monocytes after stroke, while neutralization of circulating alarmins was required to reduce systemic monocyte activation and aortic invasion. Our findings identify a synergistic effect of the sympathetic stress response and alarmin-driven inflammation via RAGE as critical mechanisms of exacerbated atheroprogression after stroke.

Introduction

The risk of recurrent vascular events after stroke is high and remains elevated even years after first stroke (*1, 2*). The enhanced risk of secondary events encompasses large artery stroke and myocardial infarction, both manifestations of atherosclerosis(*3, 4*). Atherosclerosis is a chronic inflammatory condition of the arterial vessel wall, characterized by a dysbalance in lipid metabolism and recruitment of immune cells leading to a chronic inflammatory milieu (*5, 6*). Key steps further include an infiltration by monocytes, secretion of proteolytic enzymes, fibrous cap thinning, and plaque rupture thus eventually causing end organ damage due to ischemia. Previous work in experimental myocardial infarction has demonstrated an accelerating effect of this event on atheroprogression (*7, 8*), which has recently been linked to a stress-mediated mobilization of monocytes from bone marrow niches via adrenergic signaling (*7*). The same study further provided initial evidence for accelerated atheroprogression after experimental stroke (*7*). However, the mechanisms underlying enhanced atheroprogression after stroke have so far not been investigated.

Stroke promotes a multiphasic immunomodulation in the systemic immune compartment with an early sterile inflammatory response within hours and a chronic inflammatory response that is observed both in mice and in stroke patients (*9-11*). We previously demonstrated that this systemic immunomodulation is triggered by alarmins released from necrotic brain tissue (*12*). This specifically involves the prototypic alarmin high mobility group box 1 (HMGB1). Alarmins can have chemoattractant as well as cytokine-inducing properties and interact with pattern recognition receptors such as toll-like receptors and the receptor for advanced glycation endproducts (RAGE) on various immune and non-immune cell populations (*13*).

In light of these observations, we hypothesized that stroke might promote vascular inflammation and atheroprogression via an alarmin-driven systemic immune response. In the current study, we

confirm exacerbation of atheroprogression after stroke and specifically identify a key role of the alarmin-RAGE pathway acting in synergy with the sympathetic stress response for de novo recruitment of activated monocytes to atherosclerotic lesions.

Material and Methods

Experimental design. Sample sizes were calculated using GPower 3.1. Based on a previous report (*7*) we used a monocyte increase rate of 40 % with a standard deviation of 25 %. Using an alpha-error of 0.05 and power of 0.8, we calculated a group size of 8 (t test, 2 groups, unpaired). Data was excluded from all mice, which died during surgery. Detailed exclusion criteria for the experimental models were: 1. Insufficient MCA occlusion (blood flow reduction less than 80%). 2. Death during surgery. 3. Lack of brain ischemia as quantified by histology. Animals were randomized to treatment groups and all analyses were performed by investigators blinded to group allocation. Unblinding was performed after completion of statistical analysis. All animal experiments were performed and reported in accordance with the ARRIVE guidelines (*14*).

Experimental animals. All animal experiments were performed in accordance with the guidelines for the use of experimental animals and were approved by the government committee of Upper Bavaria (Regierungspraesidium Oberbayern, #175-2013). We used age-matched, male C57BL6/J mice (8-10 weeks, 22-24g body weight, Charles River Laboratories). *ApoE*$^{-/-}$ (Jackson Laboratory) mice were fed a high-cholesterol diet (HCD, #88137, SSNIFF). Transient filament occlusion was performed in all *ApoE*$^{-/-}$ after 8 weeks of HCD. CCR2-red fluorescent protein (RFP) knock-in mice were bred with CX3CR1-GFP mice (*15*).

Statistical analysis. Data were analyzed using GraphPad Prism version 6.0. All summary data are expressed as the mean ± standard deviation. All data sets were tested for normality using the Shapiro-Wilk normality test. The groups containing normally distributed data were tested using a two-way Student's *t*-test (for 2 groups) or ANOVA (for >2 groups). The remaining data were analyzed using the Mann-Whitney *U* test (for 2 groups) or H Test (for > 2 groups). Similar variance was assured for all groups, which were statistically compared. Differences with a p

value <0.05 were considered to be statistically significant. P values were adjusted for comparison of multiple comparisons using Bonferroni correction.

Clinical stroke patient study population. Ischemic stroke patients were recruited within 24h of symptom onset. All patients had a final diagnosis of ischemic stroke as defined by an acute focal neurological deficit in combination with a diffusion weighted imaging-positive lesion on magnetic resonance imaging, or a new lesion on a delayed computed tomography scan. Age-and comorbidity-matched patients without neurological disease were used as controls. The study was approved by the local ethics committee and was conducted in accordance with the Declaration of Helsinki as well as institutional guidelines. Written and informed consent was obtained from all subjects.

More details and additional methods are described in the online Supplementary Material and Methods section.

Results

Stroke exacerbates atheroprogression via increased vascular monocyte recruitment. To determine the effect of stroke on exacerbation of atheroprogression, 8 weeks old apolipoprotein E-deficient (*ApoE*$^{-/-}$) mice(*16*), a well-established mouse model for atherosclerosis, were fed with high cholesterol diet for 8 weeks before the induction of experimental stroke and assessed plaque load after an additional 4 weeks of high cholesterol diet (**Fig. 1A**, Fig. S1). Overall plaque load in whole aorta was significantly increased in mice undergoing stroke surgery compared to sham surgery as assessed by en face staining (**Fig. 1B**). Likewise, significantly increased plaque load was observed throughout the aortic valve (**Fig. 1C-E**). Similar results were also obtained in female animals (Fig. S2). To evaluate whether stroke-induced plaque formation was accompanied by vascular inflammation, we next performed flow cytometric analysis of whole aorta cell suspensions. In contrast to other immune cell populations (Fig. S3), monocyte cell counts and more specifically the number of pro-inflammatory CD11b^{+}Ly6C^{high} monocytes per aorta was increased after stroke compared to sham (**Fig. 1F, G**). We further found a significant increase in the enzymatic activity of matrix metalloproteinases (MMP) 2 and 9 as detected by in situ zymography (**Fig. 1H, I**). Because increase of MMP activity is associated with plaque instability (*17*), we further investigated morphological markers of vulnerable plaques using previously established protocols (*18*). Cap thickness was significantly reduced and the number of highly instable plaques increased in mice undergoing stroke surgery compared to sham surgery, suggesting more vulnerable plaque morphology after stroke (**Fig. 1J**). Moreover, we analyzed plaques at the carotid bifurcation area, a predilection site for stenosis and plaque rupture in stroke patients, observing also in this area a trend towards increased plaque load after stroke (Fig S4). To determine whether the increased vascular inflammation was due to local proliferation or de novo recruitment of pro-inflammatory monocytes we next implanted osmotic pumps releasing

Bromdeoxyurdine (BrdU) for detection of cell proliferation. Additionally, we intraperitoneally (i.p.) administered $1x10^7$ $CCR2^{RFP/+}$ reporter monocytes, expressing red fluorescent protein under the CCR2 promoter, for detection of pro-inflammatory monocyte recruitment in high cholesterol diet-fed *ApoE*$^{-/-}$ mice after stroke or sham surgery (**Fig. 2A**). While we found no difference in the proliferation rate of aortic monocytes/macrophages as assessed by BrdU incorporation (**Fig. 2B**, Fig. S5), the recruitment of i.p.-injected pro-inflammatory $CCR2^{RFP/+}$ reporter cells into the aorta was substantially increased in stroke compared to sham group (**Fig. 2C, D**, Fig. S6).

Stroke induces chemoattractant expression and endothelial activation. Next, we investigated the mechanisms underlying active aortic monocyte recruitment after stroke and explored the possibility that stroke treatment may elicit a specific chemokine/cytokine profile in the atherogenic aorta. To investigate the aortic chemokine profile, we applied a PCR array for 86 chemokines and chemoattractant receptors from whole aorta lysates 3 days after stroke or sham surgery (Table S1). We found the transcription of 12 chemokines and chemoattractant receptors to be significantly upregulated after stroke compared to sham (**Fig. 2E**). Notably, the most upregulated chemokine was CCL2 with a more than 6-fold increase after stroke induction (fold change = 6.316; $p = 0.018$). CCL2 is secreted by foam cells in arterial lesions (*19*) and by activated endothelium (*20*) and attracts pro-inflammatory CCR2-expressing cells (*21-23*). Hence, we analyzed serum of stroked mice and found significantly increased CCL2 concentrations compared to sham-operated mice one week after surgery (**Fig. 2F**). In addition, monocytic CCR2 expression by flow cytometry in aortas after stroke versus sham surgery and observed a significant increase in $CCR2^+$ cell counts as well as CCR2 surface expression on inflammatory monocytes (**Fig. 2G**). One week after stroke induction we detected significantly lower aortic cell

counts of homozygous $CCR2^{RFP/RFP}$ (CCR2-deficient) compared to heterozygous $CCR2^{RFP/+}$ (CCR2-expressing) $CD11b^{+}Ly6C^{high}$ monocytes injected i.p. after stroke induction (**Fig. 2H**), indicating a critical role of the CCL2-CCR2 pathway in attraction of pro-inflammatory monocytes to the aorta after stroke.

Atherogenic monocyte recruitment is mediated by an orchestrated interplay of chemokine/chemokine receptor and integrin/adhesion molecule interactions with a pivotal role for endothelial activation. We found a significant increase mRNA expression of *Icam-1* and *Vcam-1*, key adhesion molecules in atherogenic monocyte recruitment, in aortas 3 days after stroke (**Fig. 3A**). In vivo molecular magnetic resonance imaging using micro-sized particles of iron oxide (MPIO)-labeled VCAM-1-specific antibodies (*24*) revealed a significant increase in VCAM-1 signal volume at 5 days after stroke in aortic valves compared to baseline values before stroke induction (**Fig. 3B-D**). These experiments provided strong support for the activation of the aortic endothelium after stroke. We hypothesized that the observed endothelial activation was likely mediated by soluble, pro-inflammatory mediators released from the ischemic brain as previously described by our group (*12*). To test this hypothesis, we used an in vitro endothelial culture system, subjecting murine aortic endothelial cells (MAECs) to stroke- or sham-conditioned plasma; control conditions included normal fetal calf serum (FCS)-supplemented media with or without tumor necrosis factor alpha (TNF-alpha) stimulation (**Fig. 3E**). We found mRNA expression levels of *Vcam-1*, *Icam-1* and *Il-6* significantly increased after conditioning with stroke plasma compared to sham plasma, with levels similar to stimulation of MAECs by TNF-alpha (**Fig. 3F**). Moreover, we found that addition of the soluble form of RAGE (sRAGE, 10ng/ml) decreased the expression of *Vcam-1*, *Icam-1* and *Il-6* after stimulating the MAECs with stroke plasma. These results support the concept of post-stroke endothelial activation by soluble plasma mediators such as cytokines and alarmins—druggable by decoy

receptors such as sRAGE—with an ensuing active recruitment of monocytes via CCR2-dependent pathways.

Post-stroke alarmin release induces immune activation via the RAGE signaling pathway. Acute stroke leads to massive release of pro-inflammatory alarmins such as the prototypic alarmin HMGB1 from hypoxia-stressed and necrotic tissue (*12*). We confirmed the increase of plasma HMGB1 concentrations acutely (24 hours) after experimental stroke and expanded this observation to the chronic phase (30 days) when HMGB1 plasma levels were still more than 3-fold elevated after stroke compared to sham (**Fig. 4A**). We next reduced systemic alarmins in vivo using sRAGE as a decoy receptor for circulating alarmins (*25*). We treated mice 30 minutes pre- and 4 hours post-surgical with an intraperitoneal bolus (4mg/kg) of sRAGE or vehicle and compared monocytic activation and cytokine expression in whole spleen lysates 3 days after stroke. Compared to sham-operated mice, mice undergoing stroke surgery showed an increase of major histocompatibility complex class II (MHCII) expression as a monocytic activation marker (**Fig. 4B**) and elevated levels of *Il6* and *Tnfa* mRNA (**Fig. 4C**). In contrast, sRAGE treatment abrogated the increase in MHCII expression levels and of cytokine mRNA expression after stroke (**Fig. 4B, C**). In order to investigate the role of soluble plasma mediators in monocyte activation more specifically, we treated primary monocyte cultures with recombinant HMGB1 or conditioned medium with plasma from sham operated or stroked mice. Analysis of the mRNA expression revealed an increase in *Il-6* and *Tnf-a* expression after treatment with recombinant endotoxin-free HMGB1 in a dose-dependent manner as well as plasma from stroked animals, confirming a key role for soluble mediators such as HMGB1 in the activation of monocytes (**Fig. 4D**). Accordingly, we also detected substantially increased serum HMGB1 concentrations in human stroke patients both in the acute (within first 48 h) and subacute phase (72 h and 7 days)

(**Fig. 4E,** Table S2). Analysis of the different human HMGB1 reduction/oxidation (redox) forms by mass spectroscopy identified the functionally relevant cytokine-inducing disulfide HMGB1 isoform as the predominant modification after already 3d post-stroke (**Fig. 4E**). This finding is in accordance with our previous observations on HMGB1 redox modifications in experimental stroke in mice showing that disulfide HMGB1 is the key mediator resulting in activation and expansion of the systemic monocyte population after stroke (*12, 26, 27*). Interestingly, the increase of pro-inflammatory HMGB1 was reflected in the pattern of transient leukocytosis during the time course after stroke (**Fig. 4F**). Moreover, also C reactive protein blood levels and neutrophil counts were increased post-stroke, reflecting the alarmin-driven sterile inflammatory response (Fig. S7). Accordingly, we detected a also a significant increase in the frequency of activated human leukocyte antigen ($HLA\text{-}DR^+$) cells at 2 months after human stroke (**Fig. 4G**). In light of the effective abrogation of the post-stroke systemic immune response in the presence of sRAGE, we aimed to test the effect of sRAGE treatment on stroke-induced atheroprogression. Atherosclerotic animals were treated pre- and post-surgically with an intraperitoneal bolus (4 mg/kg) of sRAGE and aortic plaque load was analyzed after sham or stroke surgery (**Fig. 5A**). We found significantly reduced plaque loads in aortas of mice receiving sRAGE compared to control-treated mice after stroke, while no difference was detected for the sham-operated groups between control and sRAGE treatment (**Fig. 5B**). Correspondingly, the overall survival rate as well as normalization of post-stroke weight loss was improved in sRAGE-treated animals (Fig. S8) and the same pattern of treatment efficacy was observed also for the plaque load in aortic valves (Fig. S9). Additionally, flow cytometric analysis revealed that sRAGE significantly abrogated the post-stroke increase in total $CD45^+CD11b^+$ monocyte as well as $CD11b^+Ly6C^{high}$ pro-inflammatory monocyte cell counts in aortas 4 weeks after stroke induction (**Fig. 5C**). Assessment of the lipid profiles of high cholesterol diet-fed $ApoE^{-/-}$ mice revealed no significant

differences after stroke induction and sRAGE treatment, except for the non-atherogenic (*28*) triglyceride levels (Fig. S10). Given the potent effect of sRAGE on neutralizing the effects of post-stroke alarmins on vascular inflammation and atheroprogression, we aimed to more specifically investigate the contribution of the RAGE-dependent pathway. To achieve specific in vivo downregulation of RAGE, we administered RAGE-specific small interfering RNA (siRNA) in HCD-fed *ApoE*$^{-/-}$ mice and found a significant knockdown of aortic RAGE mRNA expression as well as protein levels 3 days after hydrodynamic intraveneous siRNA injection of 10 nmol RAGE-silencing or negative control siRNA (**Fig. 5D, E**). siRNA-induced RAGE knockdown significantly reduced aortic total and pro-inflammatory monocyte counts 7d after stroke induction compared to control treatment with unspecific siRNA (**Fig. 5F**). As RAGE also engages ligands other than HMGB1, we next aimed to test the specific contribution of HMGB1 as a potential mediator leading to RAGE-mediated atheroprogression. Neutralizing circulating HMGB1 by intraperitoneal injection of HMGB1-specific monoclonal antibodies (4mg/kg) immediately after experimental ischemia attenuated the significant increase in cellular vascular inflammation after stroke induction (**Fig. 5G**). However, neither infarct volume nor behavioral deficits were affected one week after experimental stroke by the sRAGE or HMGB1-specific antibody treatment compared to control treatment (Figure S1). Moreover, using HMGB1-specific antibodies in WT mice reduced monocyte expansion and activation in blood and spleen 24 h after stroke (Fig. S11). To further elaborate on the role of HMGB1 as a pro-inflammatory mediator of atheroprogression, we administered recombinant HMGB1 to HCD-fed *ApoE*$^{-/-}$ mice without any surgical intervention. We found increased monocyte counts in whole aorta lysates (**Fig. 5H**) and exacerbated plaque loads in aortic valves 7d after HMGB1 injection (**Fig. 5I, J**). In addition, we detected an upregulation of *Il-6, Icam-1* and *Vcam-1* mRNA expression in whole aorta lysates (Fig. S12), resembling the pro-inflammatory expression pattern found in aortas of

mice undergoing stroke (compare to Fig. 3A). Taken together, these results indicate that HMGB1—and potentially other alarmins released from the necrotic brain tissue—induces a sterile, systemic immune response via vascular RAGE, which in turn results in exacerbation of vascular inflammation after stroke.

Alarmin release and sympathetic stress response synergize in post-stroke atheroprogression. We aimed to further dissect the differential contribution of the sympathetic innervation versus alarmin-driven cascades on the observed effects of systemic immune activation and vascular inflammation after stroke. In accord with earlier findings (*29*), we observed a decrease in overall myeloid cell count of the femur bone marrow at 24h after stroke (**Fig. 6A**). This was associated with a significant increase of tyrosine hydroxylase expression along sympathetic fibers in the femur bone marrow (**Fig. 6B, C**). These results indicated a potential release of monocytes from the bone marrow after sympathetic innervation due to a stroke-induced stress response. We and others previously observed a splenic expansion of myeloid cells after stroke induction (*12, 30*). Hence, we tested the possibility of myeloid cell trafficking from the bone marrow to the spleen after stroke using an in vivo cell tracking approach. After in vivo labeling of the bone marrow by Qdot nanocrystals—nanometer-scaled fluorophores incorporated in the cytoplasm of living cells—we found an increased number of $Qdot^+$ monocytes in spleen after stroke compared to sham surgery (**Fig. 6D, E**), while the $Qdot^+$ cell count in bone marrow decreased after stroke (Fig. S13). To further investigate the contribution of the splenic immune compartment to post-stroke vascular inflammation, we performed splenectomy versus sham surgery in HCD-fed $ApoE^{-/-}$ mice before stroke induction in both groups. Seven days after stroke, we found reduced aortic monocyte counts in splenectomized animals as well as a significantly decreased plaque load in aortic valves

compared to the non-splenectomized but stroked control group (**Fig. 6F,G**); yet, splenectomy had no effect on infarct severity or bone marrow monocyte count (Fig. S14). Taken together, these findings suggest a role of sympathetic innervation in mobilization of myeloid cells from the bone marrow niche as well as maturation/activation of monocytes in the splenic immune compartment thus contributing to stroke-induced atheroprogression. To further test this hypothesis, we analyzed the differential contribution of the alarmin signaling cascade and sympathetic innervation on monocyte cellularity and activation by using sRAGE decoy receptors and the beta3-adrenoreceptor inhibitor SR59230A (*7, 31*). Blocking beta3-adrenoreceptors but not sRAGE treatment suppressed the egress of $CD11b^+$ $CD45^+$ monocytes from the bone marrow while both treatment regimens increased overall spleen cellularity (**Fig. 6H,I**). Of note, beta3-adrenoreceptor blockage did not alter HMGB1 plasma concentrations after stroke (Fig. S15). sRAGE treatment abrogated monocyte activation in the spleen following stroke while adrenoreceptor blockage affected MHCII upregulation only when applied in combination with sRAGE (**Fig. 6J**). In blood we observed similar treatment effects with only the combination of adrenoreceptor and sRAGE blockage being effective in decreasing monocyte activation (Fig. S16). We further investigated synergistic effects of neutralizing sympathetic activation and alarmin neutralization on exacerbation of vascular inflammation after stroke. While both treatments attenuated the increase in aortic monocyte counts after stroke blocking of alarmin signaling using sRAGE was required to attenuate the increase in activated $MHCII^+$ monocytes in atherosclerotic lesions after stroke (**Fig. 6K**). We additionally analyzed the impact of adrenoreceptor and sRAGE blockage on aortic valve plaque load. In accordance with the synergistic effects of adrenoreceptor and sRAGE blockage on above-stated inflammatory markers of vascular inflammation, only the combined treatment was effective in significantly reducing aortic plaque load compared to the control treatment (**Fig. 6L**). These results suggest

that sympathetic activation during the acute stress response after stroke drives bone marrow egress of monocytic cells after stroke while brain-released alarmins are required for monocyte activation (Fig. S17).

Discussion

Large artery atherosclerosis is not only a major cause of stroke but also associated with an unexpectedly high recurrence rate (*1, 2*). We have shown that experimental stroke induces exacerbation of atheroprogression. Enhanced vascular inflammation after stroke depended on a synergistic effect of sympathetic recruitment of monocytes from the bone marrow niche and subsequent activation of innate immune and endothelial cells by circulating alarmins, attracting inflammatory monocytes to atherosclerotic lesions. We further identified the HMGB1-RAGE pathway as a critical signaling mechanism eliciting the sterile inflammatory response after stroke.

We observed a rapid translocation of bone marrow monocytes to the spleen after stroke. Myeloid monocyte mobilization has previously been shown in myocardial infarction models to be critically mediated by sympathetic signaling via beta3-adrenoreceptors (*29*). Accordingly, we showed an important role of beta3-adrenoreceptors in stroke-induced monocyte mobilization using specific inhibitors. However, while blocking sympathetic innervation attenuated monocyte evasion from the bone marrow, it did not affect monocyte activation, vascular inflammation or plaque growth. Notably, previous studies in experimental and clinical stroke have associated the sympathetic stress response with sub-acute immunosuppression but not monocyte activation or vascular inflammation (*32*). Hence, our results strengthen the concept of a second mechanism promoting the inflammatory response after stroke independent of sympathetic activation.

Aside from eliciting a local immune response with microglial activation, the release of HMGB1 and other alarmins from necrotic brain tissue induces a systemic response with cellular activation and massive cytokine secretion in peripheral immune organs (*10, 12*). Systemic immune activation involves a rapid sterile immune response acutely after stroke, followed by an immunosuppression during the subacute phase (days 2 to 7) after stroke. In addition, previous clinical studies have demonstrated a third phase characterized by a delayed chronic immune activation (from day 7 on) with elevated inflammatory markers for more than one year after stroke in patients (*9, 33*). Interestingly, the biological activity of HMGB1 depends critically on its redox state (*34, 35*). Fully-reduced HMGB1 has chemoattractant, whereas disulfide HMGB1 has cytokine-inducing properties and the terminally oxidized sulfonyl HMGB1 is anti-inflammatory (*11*). We observed that HMGB1 levels in stroke patients not only remained substantially increased during the first week after stroke but that the pro-inflammatory disulfide HMGB1 species became the predominant isoform over this time course.

Monocytes/macrophages play a critical role in the development and propagation of atherosclerotic lesions. Monocyte invasion into atherogenic lesions has been shown to be instrumental in the initiation of atherosclerosis. In this phase the chemokine-ligand receptor interaction plays a pivotal role. Studies have shown that CCR2 expression on monocytes is essential for recruitment into the adventitial space and for further plaque development (*36, 37*). In contrast, proliferation of macrophages has been demonstrated to be the key driver for lesion growth in established atherosclerosis (*38*). Surprisingly, we observed that post-stroke exacerbation of established atherosclerotic lesions was associated with enhanced de novo recruitment of circulating monocytes to the vessel rather than increased local proliferation. A possible explanation for this phenomenon is that as a consequence of the strong inflammatory response after stroke, monocyte chemoattraction via the CCL2-CCR2 axis regains a predominant

role for monocyte recruitment comparable to the initiation of the vascular inflammatory milieu (*39*). Aside from chemoattraction, endothelial expression of adhesion molecules is pivotal for monocyte recruitment. Most importantly, ICAM-1 and VCAM-1 are known to be essential for the arrest and extravasation of monocytes into the arterial wall (*40*). Our data unequivocally demonstrate the upregulation of these critical adhesion molecules on aortic endothelial cells in mice both by PCR, in vivo imaging, and in vitro cultures. In accord with our results, it was previously shown that HMGB1 is able to activate endothelial cells, leading to changes in the nuclear factors Sp-1 and NFκB, with subsequent upregulation of adhesion molecules and pro-inflammatory cytokines (*20*).

We observed a highly consistent effect of post-stroke exacerbation of atherosclerosis pathology both in female and male mice, in aortas and aortic valves, and verified this phenomenon by in vivo MRI. However, a limitation of this study is that we were not able to fully investigate the link between post-stroke atheroprogression and enhanced plaque rupture as a cause of recurrent stroke due to the limitations of the mouse atherosclerosis model. Atherosclerotic lesions of aorta and large arteries in animal models including the *ApoE*-deficient model used here, rarely develop spontaneously to destabilization and rupture with occlusive vascular thrombosis. We observed several surrogate markers of increased plaque vulnerability, however, increased incidence of plaque rupture and secondary ischemic brain lesions will have to be tested in specific models mimicking human plaque rupture and ultimately in prospective clinical studies.

In conclusion, our data identifies stroke-induced alarmin release from the ischemic brain as a critical mechanism activating inflammatory pathways and acting in synergy with an acute stress response after stroke to exacerbate atherosclerosis. Interfering with this sterile immune response by neutralizing brain-released alarmins may provide a therapeutic approach for stroke patients.

List of supplementary materials

References:

1. A. J. Grau, C. Weimar, F. Buggle, A. Heinrich, M. Goertler, S. Neumaier, J. Glahn, T. Brandt, W. Hacke, H. C. Diener, Risk factors, outcome, and treatment in subtypes of ischemic stroke: the German stroke data bank. *Stroke* **32**, 2559-2566 (2001).
2. J. Putaala, E. Haapaniemi, A. J. Metso, T. M. Metso, V. Artto, M. Kaste, T. Tatlisumak, Recurrent ischemic events in young adults after first-ever ischemic stroke. *Ann Neurol* **68**, 661-671 (2010).
3. J. K. Lovett, A. J. Coull, P. M. Rothwell, Early risk of recurrence by subtype of ischemic stroke in population-based incidence studies. *Neurology* **62**, 569-573 (2004).
4. W. B. Kannel, P. Sorlie, P. M. McNamara, Prognosis after initial myocardial infarction: the Framingham study. *Am J Cardiol* **44**, 53-59 (1979).
5. P. Libby, Inflammation in atherosclerosis. *Nature* **420**, 868-874 (2002).
6. C. Weber, H. Noels, Atherosclerosis: current pathogenesis and therapeutic options. *Nat Med* **17**, 1410-1422 (2011).
7. P. Dutta, G. Courties, Y. Wei, F. Leuschner, R. Gorbatov, C. S. Robbins, Y. Iwamoto, B. Thompson, A. L. Carlson, T. Heidt, M. D. Majmudar, F. Lasitschka, M. Etzrodt, P. Waterman, M. T. Waring, A. T. Chicoine, A. M. van der Laan, H. W. Niessen, J. J. Piek, B. B. Rubin, J. Butany, J. R. Stone, H. A. Katus, S. A. Murphy, D. A. Morrow, M. S. Sabatine, C. Vinegoni, M. A. Moskowitz, M. J. Pittet, P. Libby, C. P. Lin, F. K. Swirski, R. Weissleder, M. Nahrendorf, Myocardial infarction accelerates atherosclerosis. *Nature* **487**, 325-329 (2012).
8. A. P. Wright, M. K. Ohman, T. Hayasaki, W. Luo, H. M. Russo, C. Guo, D. T. Eitzman, Atherosclerosis and leukocyte-endothelial adhesive interactions are increased following acute myocardial infarction in apolipoprotein E deficient mice. *Atherosclerosis* **212**, 414-417 (2010).
9. J. Schulze, D. Zierath, P. Tanzi, K. Cain, D. Shibata, A. Dressel, K. Becker, Severe stroke induces long-lasting alterations of high-mobility group box 1. *Stroke* **44**, 246-248 (2013).
10. H. Offner, S. Subramanian, S. M. Parker, M. E. Afentoulis, A. A. Vandenbark, P. D. Hurn, Experimental stroke induces massive, rapid activation of the peripheral immune system. *J Cereb Blood Flow Metab* **26**, 654-665 (2006).
11. V. Singh, S. Roth, R. Veltkamp, A. Liesz, HMGB1 as a Key Mediator of Immune Mechanisms in Ischemic Stroke. *Antioxidants & redox signaling* **24**, 635-651 (2016).
12. A. Liesz, A. Dalpke, E. Mracsko, D. J. Antoine, S. Roth, W. Zhou, H. Yang, S. Y. Na, M. Akhisaroglu, T. Fleming, T. Eigenbrod, P. P. Nawroth, K. J. Tracey, R. Veltkamp, DAMP signaling is a key pathway inducing immune modulation after brain injury. *The Journal of neuroscience : the official journal of the Society for Neuroscience* **35**, 583-598 (2015).
13. J. Li, R. Kokkola, S. Tabibzadeh, R. Yang, M. Ochani, X. Qiang, H. E. Harris, C. J. Czura, H. Wang, L. Ulloa, H. Wang, H. S. Warren, L. L. Moldawer, M. P. Fink, U. Andersson, K. J. Tracey, H. Yang, Structural basis for the proinflammatory cytokine activity of high mobility group box 1. *Mol Med* **9**, 37-45 (2003).
14. C. Kilkenny, W. J. Browne, I. C. Cuthill, M. Emerson, D. G. Altman, Improving bioscience research reporting: the ARRIVE guidelines for reporting animal research. *PLoS Biol* **8**, e1000412 (2010).
15. N. Saederup, A. E. Cardona, K. Croft, M. Mizutani, A. C. Cotleur, C. L. Tsou, R. M. Ransohoff, I. F. Charo, Selective chemokine receptor usage by central nervous system myeloid cells in CCR2-red fluorescent protein knock-in mice. *PLoS One* **5**, e13693 (2010).
16. A. S. Plump, J. D. Smith, T. Hayek, K. Aalto-Setala, A. Walsh, J. G. Verstuyft, E. M. Rubin, J. L. Breslow, Severe hypercholesterolemia and atherosclerosis in apolipoprotein E-deficient mice created by homologous recombination in ES cells. *Cell* **71**, 343-353 (1992).
17. J. L. Johnson, A. H. Baker, K. Oka, L. Chan, A. C. Newby, C. L. Jackson, S. J. George, Suppression of atherosclerotic plaque progression and instability by tissue inhibitor of metalloproteinase-2: involvement of macrophage migration and apoptosis. *Circulation* **113**, 2435-2444 (2006).
18. J. Johnson, K. Carson, H. Williams, S. Karanam, A. Newby, G. Angelini, S. George, C. Jackson, Plaque rupture after short periods of fat feeding in the apolipoprotein E-knockout mouse: model characterization and effects of pravastatin treatment. *Circulation* **111**, 1422-1430 (2005).
19. K. J. Moore, F. J. Sheedy, E. A. Fisher, Macrophages in atherosclerosis: a dynamic balance. *Nat Rev Immunol* **13**, 709-721 (2013).
20. C. Fiuza, M. Bustin, S. Talwar, M. Tropea, E. Gerstenberger, J. H. Shelhamer, A. F. Suffredini, Inflammation-promoting activity of HMGB1 on human microvascular endothelial cells. *Blood* **101**, 2652-2660 (2003).

21. C. L. Tsou, W. Peters, Y. Si, S. Slaymaker, A. M. Aslanian, S. P. Weisberg, M. Mack, I. F. Charo, Critical roles for CCR2 and MCP-3 in monocyte mobilization from bone marrow and recruitment to inflammatory sites. *J Clin Invest* **117**, 902-909 (2007).
22. C. Shi, E. G. Pamer, Monocyte recruitment during infection and inflammation. *Nat Rev Immunol* **11**, 762-774 (2011).
23. P. Dutta, H. B. Sager, K. R. Stengel, K. Naxerova, G. Courties, B. Saez, L. Silberstein, T. Heidt, M. Sebas, Y. Sun, G. Wojtkiewicz, P. F. Feruglio, K. King, J. N. Baker, A. M. van der Laan, A. Borodovsky, K. Fitzgerald, M. Hulsmans, F. Hoyer, Y. Iwamoto, C. Vinegoni, D. Brown, M. Di Carli, P. Libby, S. W. Hiebert, D. T. Scadden, F. K. Swirski, R. Weissleder, M. Nahrendorf, Myocardial Infarction Activates CCR2(+) Hematopoietic Stem and Progenitor Cells. *Cell stem cell* **16**, 477-487 (2015).
24. M. Gauberti, A. Montagne, O. A. Marcos-Contreras, A. Le Behot, E. Maubert, D. Vivien, Ultra-sensitive molecular MRI of vascular cell adhesion molecule-1 reveals a dynamic inflammatory penumbra after strokes. *Stroke* **44**, 1988-1996 (2013).
25. L. Park, K. G. Raman, K. J. Lee, Y. Lu, L. J. Ferran, Jr., W. S. Chow, D. Stern, A. M. Schmidt, Suppression of accelerated diabetic atherosclerosis by the soluble receptor for advanced glycation endproducts. *Nat Med* **4**, 1025-1031 (1998).
26. H. Offner, S. Subramanian, S. M. Parker, C. Wang, M. E. Afentoulis, A. Lewis, A. A. Vandenbark, P. D. Hurn, Splenic atrophy in experimental stroke is accompanied by increased regulatory T cells and circulating macrophages. *J Immunol* **176**, 6523-6531 (2006).
27. A. Hug, A. Dalpke, N. Wieczorek, T. Giese, A. Lorenz, G. Auffarth, A. Liesz, R. Veltkamp, Infarct volume is a major determiner of post-stroke immune cell function and susceptibility to infection. *Stroke* **40**, 3226-3232 (2009).
28. B. G. Talayero, F. M. Sacks, The role of triglycerides in atherosclerosis. *Current cardiology reports* **13**, 544-552 (2011).
29. G. Courties, F. Herisson, H. B. Sager, T. Heidt, Y. Ye, Y. Wei, Y. Sun, N. Severe, P. Dutta, J. Scharff, D. T. Scadden, R. Weissleder, F. K. Swirski, M. A. Moskowitz, M. Nahrendorf, Ischemic stroke activates hematopoietic bone marrow stem cells. *Circ Res* **116**, 407-417 (2015).
30. M. Nahrendorf, M. J. Pittet, F. K. Swirski, Monocytes: protagonists of infarct inflammation and repair after myocardial infarction. *Circulation* **121**, 2437-2445 (2010).
31. Y. Katayama, M. Battista, W. M. Kao, A. Hidalgo, A. J. Peired, S. A. Thomas, P. S. Frenette, Signals from the sympathetic nervous system regulate hematopoietic stem cell egress from bone marrow. *Cell* **124**, 407-421 (2006).
32. A. Chamorro, A. Meisel, A. M. Planas, X. Urra, D. van de Beek, R. Veltkamp, The immunology of acute stroke. *Nature reviews. Neurology* **8**, 401-410 (2012).
33. A. Liesz, H. Ruger, J. Purrucker, M. Zorn, A. Dalpke, M. Mohlenbruch, S. Englert, P. P. Nawroth, R. Veltkamp, Stress mediators and immune dysfunction in patients with acute cerebrovascular diseases. *PLoS One* **8**, e74839 (2013).
34. D. J. Antoine, H. E. Harris, U. Andersson, K. J. Tracey, M. E. Bianchi, A systematic nomenclature for the redox states of high mobility group box (HMGB) proteins. *Mol Med*, (2014).
35. E. Venereau, M. Casalgrandi, M. Schiraldi, D. J. Antoine, A. Cattaneo, F. De Marchis, J. Liu, A. Antonelli, A. Preti, L. Raeli, S. S. Shams, H. Yang, L. Varani, U. Andersson, K. J. Tracey, A. Bachi, M. Uguccioni, M. E. Bianchi, Mutually exclusive redox forms of HMGB1 promote cell recruitment or proinflammatory cytokine release. *J Exp Med* **209**, 1519-1528 (2012).
36. L. Boring, J. Gosling, M. Cleary, I. F. Charo, Decreased lesion formation in CCR2-/- mice reveals a role for chemokines in the initiation of atherosclerosis. *Nature* **394**, 894-897 (1998).
37. J. Guo, M. Van Eck, J. Twisk, N. Maeda, G. M. Benson, P. H. Groot, T. J. Van Berkel, Transplantation of monocyte CC-chemokine receptor 2-deficient bone marrow into ApoE3-Leiden mice inhibits atherogenesis. *Arteriosclerosis, thrombosis, and vascular biology* **23**, 447-453 (2003).
38. C. S. Robbins, I. Hilgendorf, G. F. Weber, I. Theurl, Y. Iwamoto, J. L. Figueiredo, R. Gorbatov, G. K. Sukhova, L. M. Gerhardt, D. Smyth, C. C. Zavitz, E. A. Shikatani, M. Parsons, N. van Rooijen, H. Y. Lin, M. Husain, P. Libby, M. Nahrendorf, R. Weissleder, F. K. Swirski, Local proliferation dominates lesional macrophage accumulation in atherosclerosis. *Nat Med* **19**, 1166-1172 (2013).
39. B. Coll, C. Alonso-Villaverde, J. Joven, Monocyte chemoattractant protein-1 and atherosclerosis: is there room for an additional biomarker? *Clinica chimica acta; international journal of clinical chemistry* **383**, 21-29 (2007).
40. J. Cros, N. Cagnard, K. Woollard, N. Patey, S. Y. Zhang, B. Senechal, A. Puel, S. K. Biswas, D. Moshous, C. Picard, J. P. Jais, D. D'Cruz, J. L. Casanova, C. Trouillet, F. Geissmann, Human CD14dim monocytes patrol and sense nucleic acids and viruses via TLR7 and TLR8 receptors. *Immunity* **33**, 375-386 (2010).

Acknowledgments: The authors thank Kerstin Thuß-Silczak for excellent technical assistance and Dr. Urban Deutsch for maintaining transgenic mouse colonies at the University of Bern. $CCR2^{RFP/RFP}CX3CR1^{GFP/+}$ mice were kindly donated by Israel F. Charo (University of California, San Francisco, USA) and Richard Ransohoff (Biogen Idec, Boston, USA). sRAGE baculovirus was a kind donation by Ann-Marie Schmidt (New York University Langone Medical Center, New York City, USA).

Funding: This study was funded by the excellence cluster of the German research foundation "Munich Cluster for Systems Neurology (SyNergy)" EXC1010 to M.D., A.L. and J.B., and the German Research Foundation
(DFG, LI-2534/2-1) to A.L., (SFB1123-A03) to J.B. and (SFB1123-B01) L.M.H.

Author contributions: SR performed experiments, analyzed data and wrote the manuscript; VS, ST, LS, GH, DJA, AA, CO, MG, AF, MEB, LH performed experiments and analyzed data; contribution of individual scientists to performing and analyzing specific experiments is defined in Table S4; AG, DV, HEH, BE, MEB contributed critical material and techniques for this study; CH, JB, MD contributed critical input to study design and manuscript writing; AL initiated and coordinated the study, analyzed data and wrote the manuscript.

Disclosures: All authors state that they have no competing interest in relation to the presented study.

Figure 1. Stroke exacerbates atheroprogression.

(**A**) Experimental design: *ApoE*$^{-/-}$ mice fed with high cholesterol diet (HCD-fed *ApoE*$^{-/-}$) underwent stroke or sham surgery and were sacrificed one month after surgical procedure. (**B**) Representative whole aorta en face Oil Red O staining in sham and stroked mice (left) and quantification of the plaque load one month after stroke in sham and stroked animals (U Test, n= 8 per group). **(C)** Representative images of Oil Red O stained aortic valve sections one month after stroke or sham surgery. (**D**) Schematic representation of aortic valve. Red lines indicate the location of the sections analyzed in the study. (**E**) Quantification of aortic valve plaque load shown as percentage of plaque area per aortic valve in each section shown in b (left) and the area under the curve (right, U Test, n= 12 per group). (**F**) Representative gating strategy for flow cytometric analysis of aortic monocytes. (**G**) Flow cytometric analysis of whole aorta lysates showing total monocytes (CD11b^{+}; left) and the pro-inflammatory subset (Ly6C^{high}; right) cell counts after stroke induction compared to sham (U Test, n= 9-10 per group). (**H**) Representative images of aortic valve in situ zymography for DAPI (neuronal marker, blue) and MMP2/9 (representing enzymatically active areas, green) one month after surgery. (**I**) Quantification of MMP2/9 activity showed as enzymatically active area and normalized intensity (U Test, n=12 per group). (**J**) Representative images of Oil Red O stained aortic valve sections one month after stroke (left) and quantification of number of plaque ruptures and cap thickness in aortic valve sections one month after sham or stroke surgery. (U Test, n= 14-15 per group). The arrowhead in the high magnification image indicates a buried fibrous cap in lesion.

Figure 2. Stroke increases vascular inflammation via recruitment of inflammatory monocytes to atherosclerotic plaques. (**A**) Schematic illustration of experimental design for data shown in b-d: HCD-fed *ApoE*$^{-/-}$ mice underwent sham or stroke surgery and received either continuous BrdU administration or RFP^{+}CCR2^{+} bone marrow-derived cells (BMDCs) i.p. After one week, mice were sacrificed and aortas and lymphoid organs were analyzed. (**B**) Analysis of BrdU^{+}CD11b^{+} monocytes from aortas after stroke or sham surgery (U Test, n= 5-7 per group). (**C**) Gating strategy and representative histogram plots (right) for invading RFP^{+} monocytes in aortas (grey= sham, white= stroke) and (**D**) corresponding quantification of RFP^{+}CD11b^{+} monocytes in aorta (U Test, n= 5-6 per group). (**E**) Fold change and adjusted p values (in brackets) of chemokine and chemokine receptor transcription after stroke compared to sham aorta lysates 3 days after surgery (left panel, n= 3 per group, p value <0.1) and corresponding volcano plot for transcriptional regulation determined by rtPCR arrays (right panel; x-axis= fold change; y-axis= p value, cut-off at <0.1). (**F**) Serum levels of CCL2 one week after stroke compared to sham surgery (U Test, n= 4-6 per group). (**G**) Flow cytometric analysis of aortic CCR2^{+}Ly6C^{high} monocytes (left) as well as CCR2^{+} surface expression on inflammatory Ly6C^{high} monocytes (right) in aortas 3 days after stroke or sham-surgery (U Test, n= 7 per group). (**H**) Quantification of aortic invasion of adoptively transferred RFP-reporter cells from either CCR2-deficient (CCR2$^{RFP/RFP}$) or –positive RFP^{+} donor mice (CCR2$^{RFP/+}$) (U Test, n= 5-6 per group).

Figure 3. Stroke induces inflammatory activation of the aortic endothelium. (**A**) Relative expression (RE) of *Icam1* and *Vcam1* transcription in whole aorta lysates 3 days after sham or stroke (U Test, n= 5 per group). (**B**) VCAM-1-targeted iron particles were used for molecular MR imaging of endothelial activation in vivo before and after stroke. Representative longitudinal and sagittal MRI images of aortic root area 5 days after stroke. (**C**) Representative comparison of the VCAM-1 signal volume of the same aortic valve before and 5 days after stroke surgery (see methods for details). (**D**) Quantification of VCAM-1 signal volume 5 days after stroke compared to baseline (U Test, n= 5). (**E**) Schematic illustration of experiments shown in (**F**). WT mice received either stroke or sham surgery; 4 h later plasma was collected and used for conditioning media in murine aortic endothelial cell (MAEC) cultures. (**F**) Relative expression (RE) of *Icam1, Vcam1* and *Il6* mRNA in MAEC after being either incubated with stroke or sham plasma and treated with sRAGE (10 ng/ml) or vehicle (H Test, n= 6-8). For control conditions, fetal calf serum (FCS) supplemented media without cytokine stimulus or with 20 ng/ml recombinant TNF-α (TNF- α) were used. *: $p < 0.05$, **: $p < 0.01$, ***: $p < 0.001$.

Figure 4. HMGB1 induces systemic innate immune activation after stroke. (**A**) Plasma HMGB1 concentrations were measured by ELISA in naïve, sham and stroke operated HCD-fed *ApoE*$^{-/-}$ mice 1 day and 30 days after surgery (One way-ANOVA, n= 7-9 per group). (**B**) Flow cytometric analysis of splenic myeloid cells from HCD-fed *ApoE*$^{-/-}$ mice (CD45^{+}CD11b^{+}) revealed elevated MHCII^{+} expression 3 days after stroke with vehicle or sRAGE treatment (One way-ANOVA, n= 8 per group). (**C**) Relative expression (RE) of *Il6* and *Tnfa* mRNA in spleen of sham operated and stroked vehicle treated or sRAGE treated WT mice 3 days after surgical procedure (H Test, n= 6 per group). (**D**) Relative expression of *Il6* and *Tnfa* mRNA of isolated murine splenic monocytes from WT mice which were stimulated with recombinant HMGB1 (0.1 and 0.5 µg/ml), murine sham and stroke plasma (50 %) and LPS (0.1 µg/ml) in vitro (H Test, n= 5-8 per group). (**E**) Plasma concentration of HMGB1 acquired by quantitative mass spectrometry analysis at different time points (day 1 – day 7) in stroke patients and age-matched controls (HC, left panel, n=15-18 per group, One way-ANOVA). Changes in the distribution of HMGB1 redox state from fully reduced to disulfide state over the first week after stroke (right panel, n=15-18 per group). (**F**) Quantification of blood leukocyte counts in stroke and control patients (n=15-18 per group). (**G**) Flow cytometric analysis of human patient blood samples for HLA-DR^{+} cell count as an indication for monocyte activation at up to 60 days after large ischemic stroke compared to age-matched controls (t test, n= 12-17 per group). *: $p < 0.05$, **: $p < 0.01$, ***: $p < 0.001$.

Figure 5. Stroke induces atheroprogression via the RAGE-signaling pathway. (**A**) Schematic illustration of experimental design for data shown in panel b-d: HCD-fed *ApoE*$^{-/-}$ mice received either an i.p. injection of sRAGE or vehicle treatment 30 min before and 4 h after the respective surgery and were sacrificed one month later. (**B**) Quantification of the overall plaque area per aorta in stroke or sham mice treated with sRAGE or vehicle one month after surgery (ANOVA, n= 8 per group). (**C**) Flow cytometric analysis of whole aorta for CD11b^{+} and CD11b^{+}Ly6C^{high} monocyte counts after stroke with sRAGE or vehicle treatment compared to sham-operated mice one month after surgery (H Test, n= 7-8 per group). (**D**) RAGE mRNA expression 3 days after hydrodynamic intraveneous injection of RAGE-specific small interfering RNA (siRNA) or control siRNA (ctrl, U Test, n= 5 per group) (**E**) Correspondingly, RAGE protein levels 3 days after RAGE-specific or control siRNA injection (n= 3 per group). (**F**) HCD-fed *ApoE*$^{-/-}$ mice received stroke or sham surgery 3 days after hydrodynamic RAGE-specific or control siRNA injection and were sacrificed 7 days later for flow cytometric analysis of whole aortas for CD11b^{+} and CD11b^{+}Ly6C^{high} monocyte counts (H Test, n= 5-6 per group). (**G**) Mice received HMGB1-specific or control IgG antibodies immediately after surgery (sham or stroke) and CD11b^{+} and CD11b^{+}Ly6C^{high} monocytes counts were analyzed with flow cytometry 7 days later. (H Test, n= 5-6 per group). (**H**) Flow cytometric analysis for CD11b^{+} and CD11b^{+}Ly6C^{high} monocyte counts of whole aortas 7 days after an intraperitoneal injection of vehicle or rHMGB1 to HCD-fed *ApoE*$^{-/-}$ mice. (U Test, n= 7-8 per group). (**I**) Representative images of Oil Red O stained aortic valve sections 7 days after rHMGB1 administration. (**J**) Comparison of Oil Red O^{+} area on five consecutive levels in aortic valves (left). Area under curve analysis of the individual aortic valves (right) after HMGB1 administration compared to control treated naïve *ApoE*$^{-/-}$ mice (U Test, n= 7 per group). *: $p < 0.05$, **: $p < 0.01$.

Figure 6. Alarmin release and sympathetic stress response synergize in post-stroke atheroprogression. (**A**) Flow cytometric analysis of myeloid cellularity in femur bone marrow 24 h after stroke compared to sham surgery. (**B**) Representative images of immunofluorescence staining for tyrosine hydroxylase (TH) in femoral bone marrow 24 h after stroke and sham surgery. (**C**) Quantification of TH^+ area after stroke compared to sham on femoral sections (U Test, n= 7 per group). (**D**) WT mice received Qdot nanocrystal injections in the femoral bone marrow 2 h before stroke or sham surgery and were sacrificed 24 h later (U Test, n= 6 per group). Representative gating strategy for $CD45^+CD11b^+$ monocytes and $Qdot^+$ myeloid cells in spleen after stroke or sham surgery. (**E**) Quantification of total $Qdot^+$ myeloid cells in spleens after stroke compared to sham surgery (right panel; U Test, n= 5 per group). (**F**) HCD-fed *ApoE*$^{-/-}$ mice were splenectomized before stroke or sham surgery (see methods for details) and analyzed 7 days after stroke for total monocyte cell counts and pro-inflammatory $Ly6C^{high}$ frequency in aortas one week after stroke. (**G**) Quantification of overall plaque area in aortic valves of splenectomized mice after stroke induction (U Test, n= 6-8 per group). WT mice received either sRAGE, $ß_3$-blocker SR59230, both combined or control treatment immediately after stroke and bone marrow (**H**) and spleen (**I, J**) were analyzed by flow cytometry 24 h later for the total myeloid ($CD45^+CD11b^+$) cell count and monocyte activation (percentage of $MHCII^+$ monocytes; H Test, n= 6-8 per group). (**K**) HCD-fed *ApoE*$^{-/-}$ mice received sRAGE, SR59230, combination therapy or control treatment immediately after stroke. Bar graphs represent the flow cytometric analysis of $CD45^+CD11b^+$ monocyte cell count, the percentage of $MHCII^+$ monocytes and $Ly6C^{high}$ monocytes in aortas one week after stroke (H Test, n= 7-8 per group). (**L**) Quantification of plaque load in five consecutive levels of aortic valve and Area under curve analysis for HCD-fed *ApoE*$^{-/-}$ mice (H Test, n= 5-6 per group). *: $p < 0.05$, **: $p < 0.01$.

Figure 1

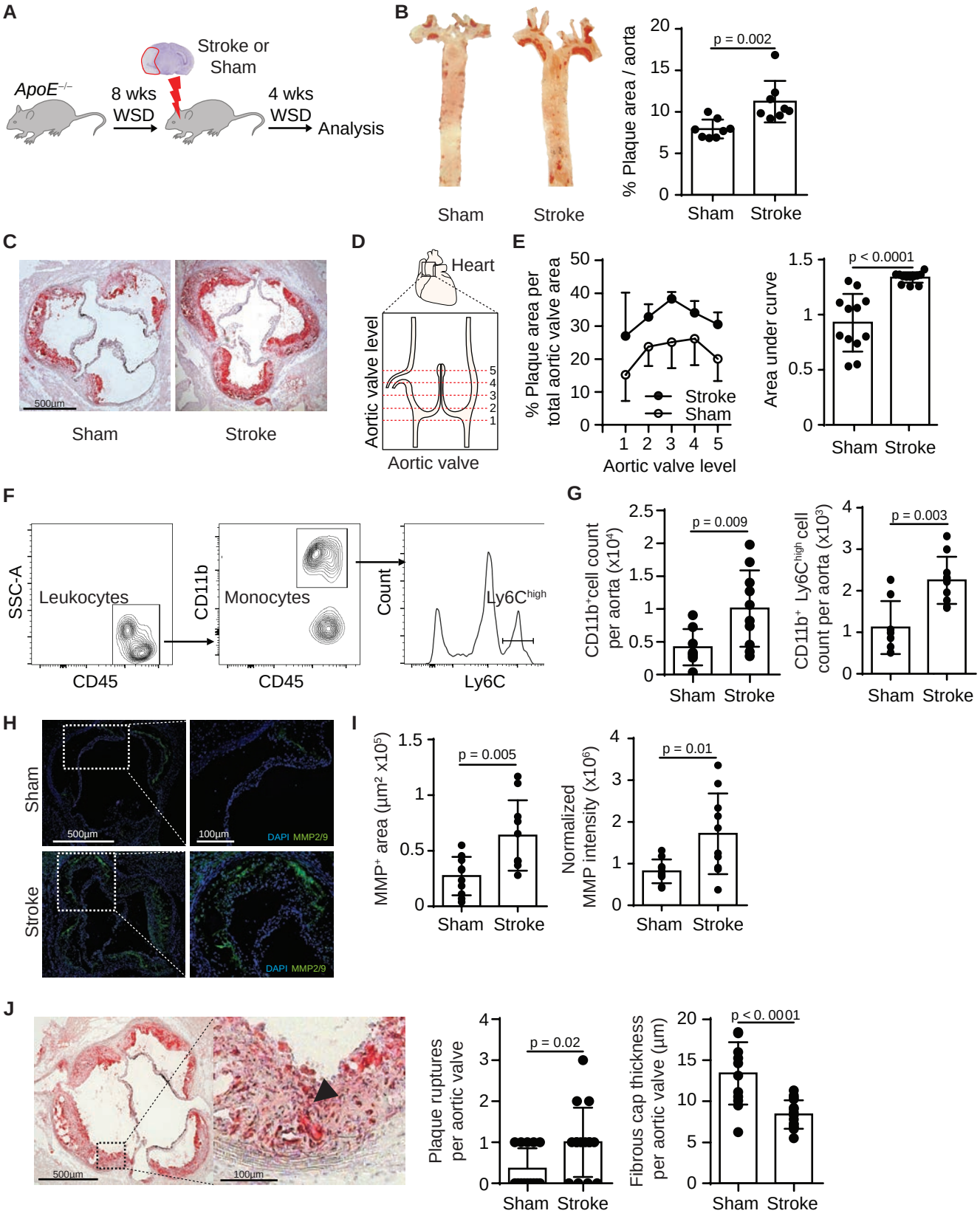
A
ApoE−/−
8 wks WSD
Stroke or Sham
4 wks WSD
Analysis
B
Sham
Stroke
% Plaque area / aorta
p = 0.002
C
500µm
Sham
Stroke
D
Heart
Aortic valve level
Aortic valve
E
% Plaque area per total aortic valve area
Stroke
Sham
Aortic valve level
Area under curve
p < 0.0001
F
SSC-A
Leukocytes
CD45
CD11b
Monocytes
CD45
Count
Ly6Chigh
Ly6C
G
CD11b+cell count per aorta (x10⁴)
p = 0.009
CD11b+ Ly6Chigh cell count per aorta (x10³)
p = 0.003
H
Sham
Stroke
500µm
100µm
DAPI MMP2/9
I
MMP+ area (µm² x10⁵)
p = 0.005
Normalized MMP intensity (x10⁶)
p = 0.01
J
500µm
100µm
Plaque ruptures per aortic valve
p = 0.02
Fibrous cap thickness per aortic valve (µm)
p < 0.0001

Figure 2

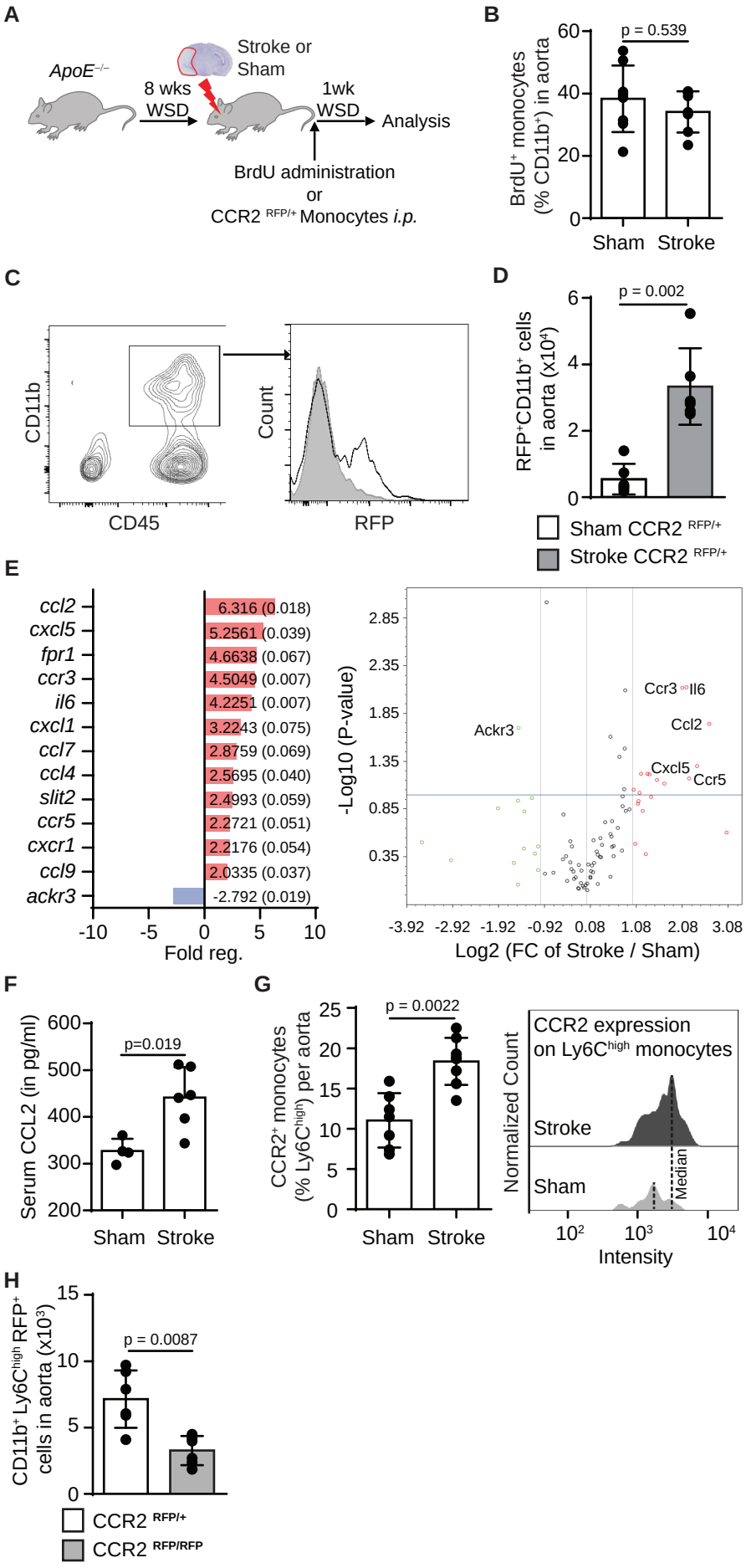
A
ApoE−/−
8 wks WSD
Stroke or Sham
1wk WSD
Analysis
BrdU administration or CCR2 RFP/+ Monocytes i.p.
B
p = 0.539
BrdU+ monocytes (% CD11b+) in aorta
Sham
Stroke
C
CD11b
CD45
Count
RFP
D
p = 0.002
RFP+CD11b+ cells in aorta (x10⁴)
Sham CCR2 RFP/+
Stroke CCR2 RFP/+
E
ccl2 6.316 (0.018)
cxcl5 5.2561 (0.039)
fpr1 4.6638 (0.067)
ccr3 4.5049 (0.007)
il6 4.2251 (0.007)
cxcl1 3.2243 (0.075)
ccl7 2.8759 (0.069)
ccl4 2.5695 (0.040)
slit2 2.4993 (0.059)
ccr5 2.2721 (0.051)
cxcr1 2.2176 (0.054)
ccl9 2.0335 (0.037)
ackr3 -2.792 (0.019)
Fold reg.
-Log10 (P-value)
Ackr3
Ccr3
Il6
Ccl2
Cxcl5
Ccr5
Log2 (FC of Stroke / Sham)
F
p=0.019
Serum CCL2 (in pg/ml)
Sham
Stroke
G
p = 0.0022
CCR2+ monocytes (% Ly6Chigh) per aorta
CCR2 expression on Ly6Chigh monocytes
Stroke
Sham
Median
Normalized Count
Intensity
H
p = 0.0087
CD11b+ Ly6Chigh RFP+ cells in aorta (x10³)
CCR2 RFP/+
CCR2 RFP/RFP

Figure 3

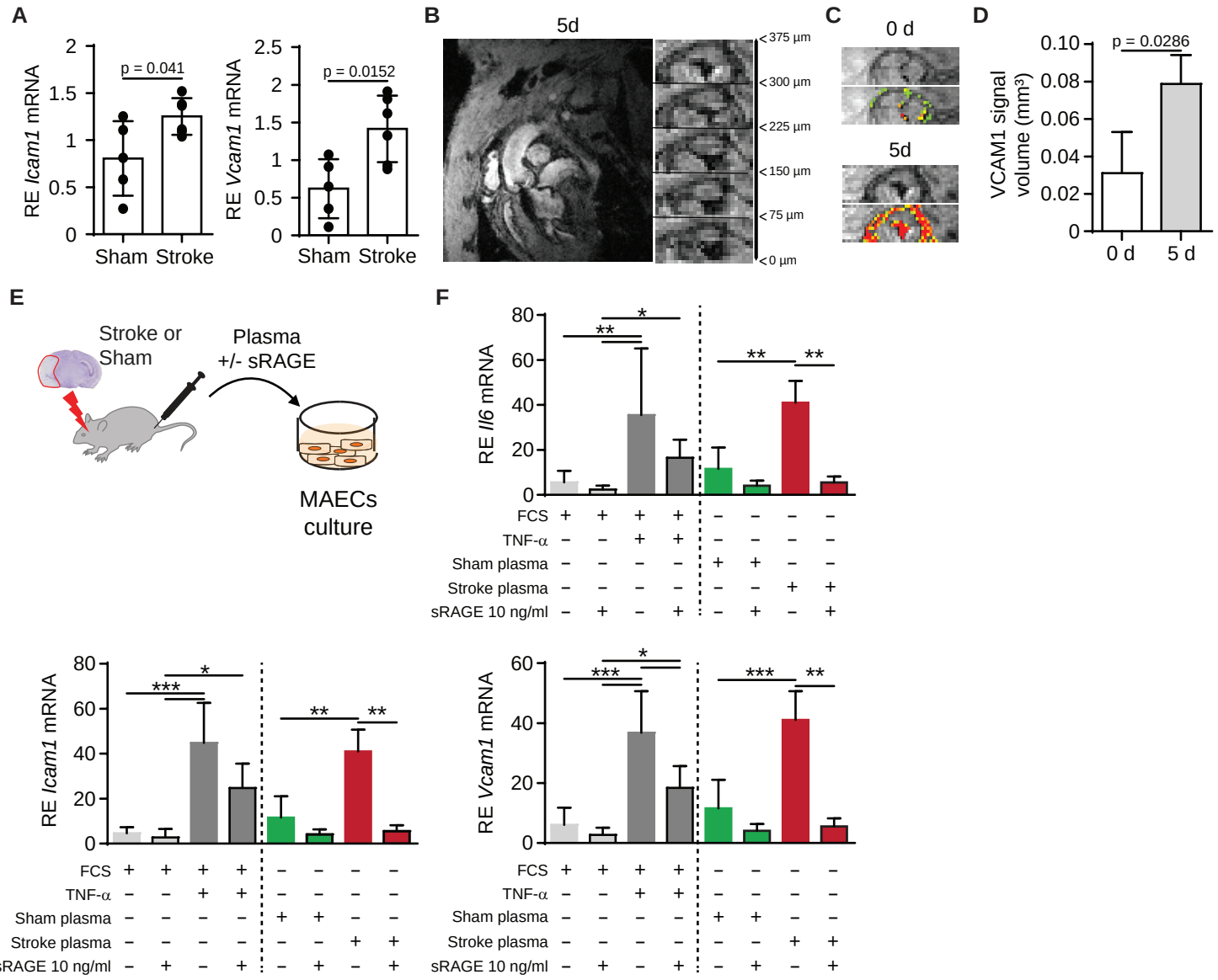
A
RE Icam1 mRNA
p = 0.041
Sham Stroke
RE Vcam1 mRNA
p = 0.0152
Sham Stroke
B
5d
375 µm
300 µm
225 µm
150 µm
75 µm
0 µm
C
0 d
5d
D
VCAM1 signal volume (mm³)
p = 0.0286
0 d
5 d
E
Stroke or Sham
Plasma +/- sRAGE
MAECs culture
F
RE Il6 mRNA
FCS
TNF-α
Sham plasma
Stroke plasma
sRAGE 10 ng/ml
RE Icam1 mRNA
RE Vcam1 mRNA

Figure 4

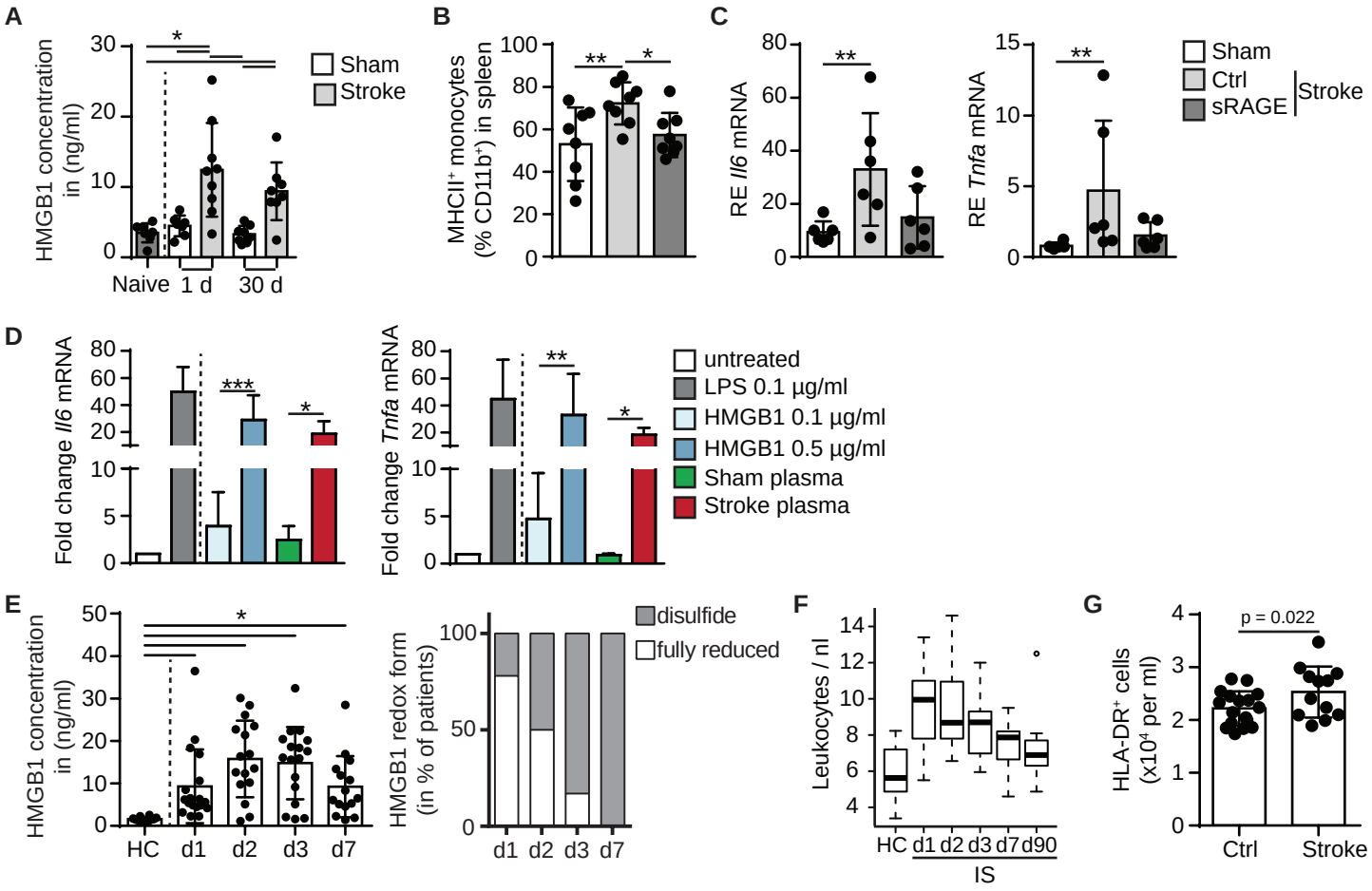
A
HMGB1 concentration in (ng/ml)
Sham
Stroke
Naive
1 d
30 d
B
MHCII+ monocytes (% CD11b+) in spleen
C
RE Il6 mRNA
RE Tnfa mRNA
Sham
Ctrl
sRAGE
Stroke
D
Fold change Il6 mRNA
Fold change Tnfa mRNA
untreated
LPS 0.1 µg/ml
HMGB1 0.1 µg/ml
HMGB1 0.5 µg/ml
Sham plasma
Stroke plasma
E
HMGB1 concentration in (ng/ml)
HC
d1
d2
d3
d7
HMGB1 redox form (in % of patients)
disulfide
fully reduced
F
Leukocytes / nl
HC
d1
d2
d3
d7
d90
IS
G
HLA-DR+ cells (x10⁴ per ml)
p = 0.022
Ctrl
Stroke

Figure 5

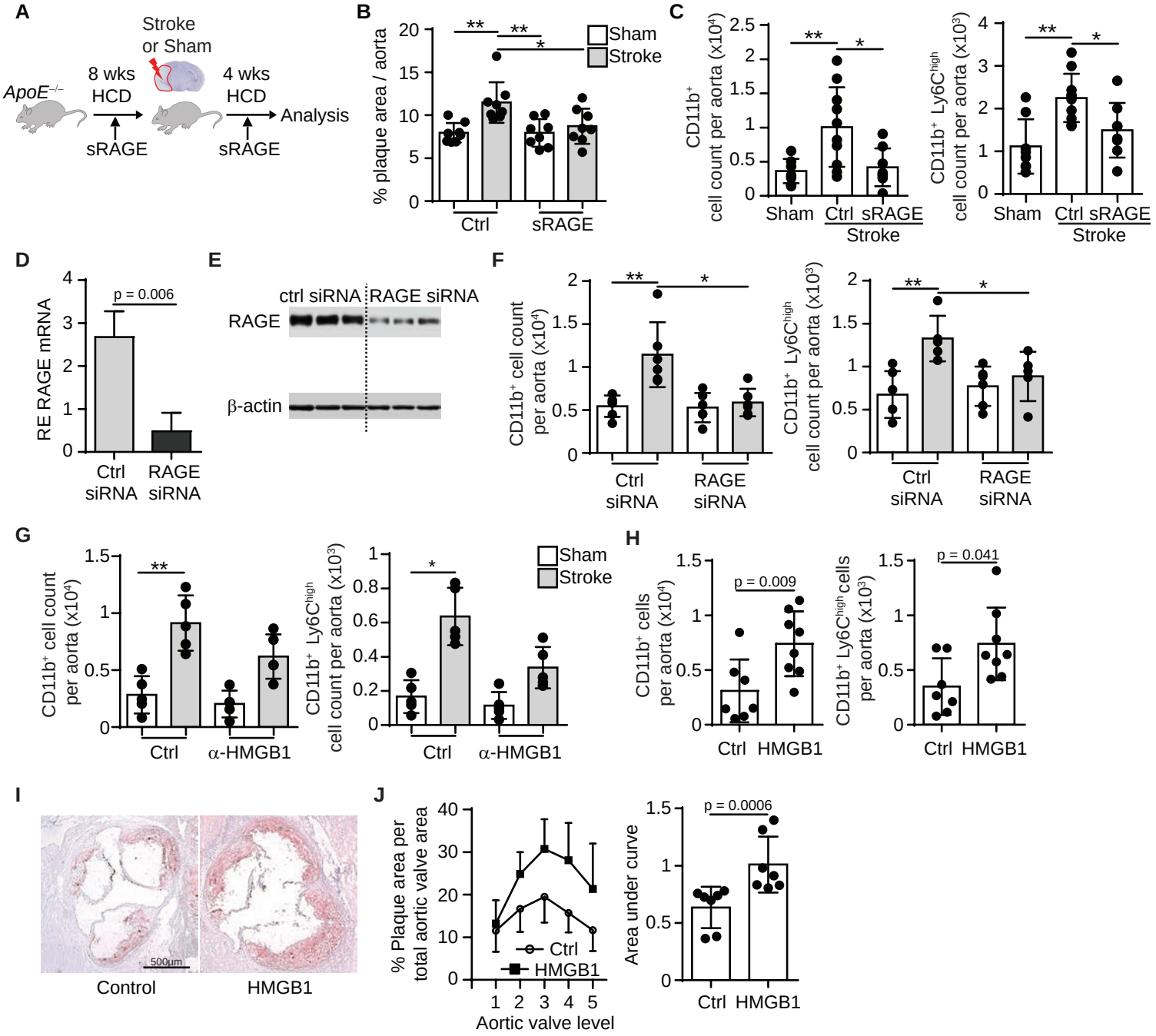
A
Stroke
or Sham
ApoE−/−
8 wks
HCD
4 wks
HCD
Analysis
sRAGE
sRAGE
B
% plaque area / aorta
Sham
Stroke
Ctrl
sRAGE
C
CD11b+ cell count per aorta (x10⁴)
CD11b+ Ly6Chigh cell count per aorta (x10³)
Sham
Ctrl
sRAGE
Stroke
D
RE RAGE mRNA
p = 0.006
Ctrl siRNA
RAGE siRNA
E
ctrl siRNA
RAGE siRNA
RAGE
β-actin
F
CD11b+ cell count per aorta (x10⁴)
CD11b+ Ly6Chigh cell count per aorta (x10³)
Ctrl siRNA
RAGE siRNA
G
CD11b+ cell count per aorta (x10⁴)
CD11b+ Ly6Chigh cell count per aorta (x10³)
Sham
Stroke
Ctrl
α-HMGB1
H
CD11b+ cells per aorta (x10⁴)
CD11b+ Ly6Chigh cells per aorta (x10³)
p = 0.009
p = 0.041
Ctrl
HMGB1
I
500µm
Control
HMGB1
J
% Plaque area per total aortic valve area
Ctrl
HMGB1
Aortic valve level
Area under curve
p = 0.0006
Ctrl
HMGB1

Figure 6

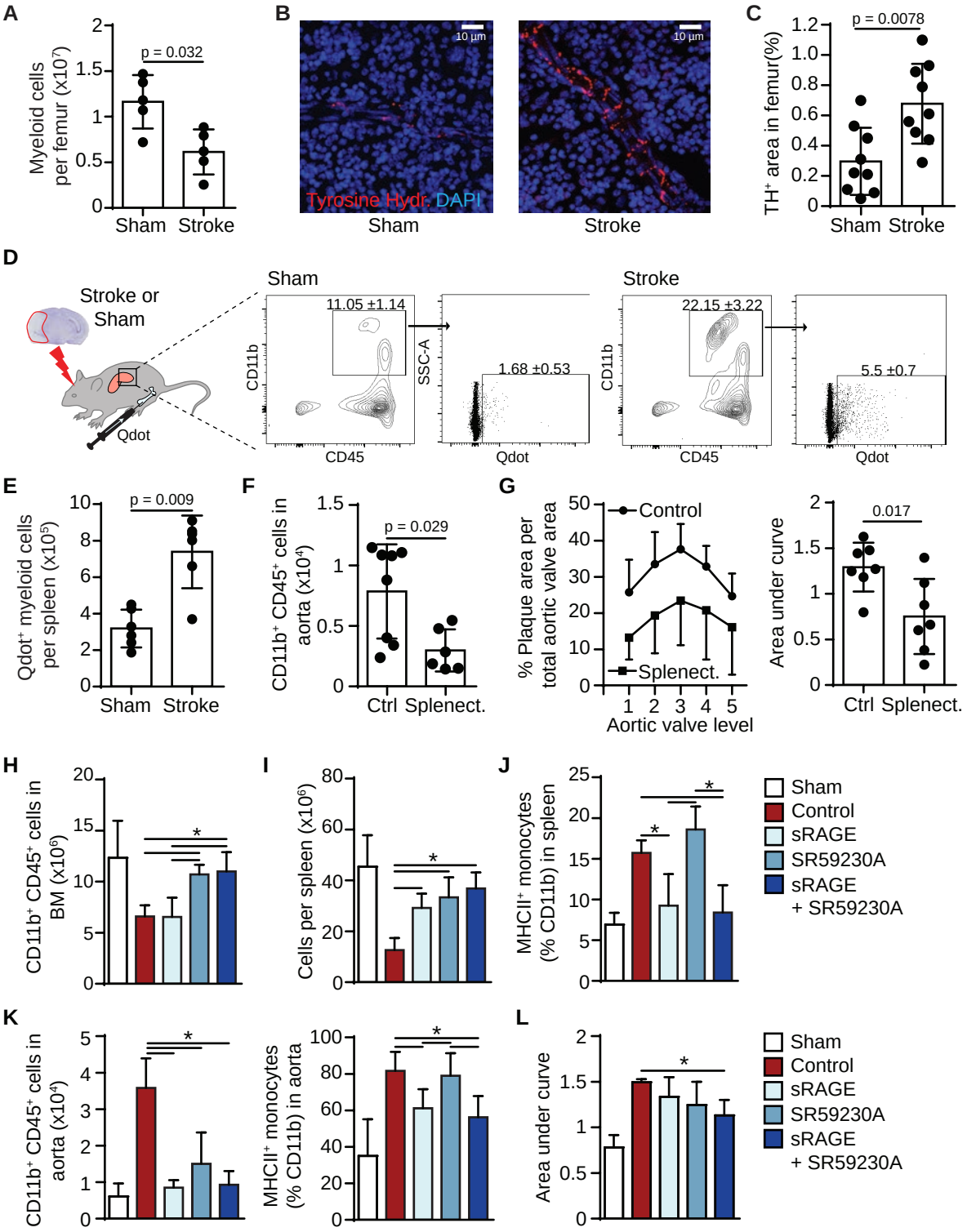
A
Myeloid cells per femur (x10^7)
p = 0.032
Sham Stroke
B
10 µm
Tyrosine Hydr. DAPI
Sham
Stroke
C
TH+ area in femur(%)
p = 0.0078
Sham Stroke
D
Stroke or Sham
Qdot
Sham
11.05 ±1.14
1.68 ±0.53
CD11b
SSC-A
CD45
Qdot
Stroke
22.15 ±3.22
5.5 ±0.7
E
Qdot+ myeloid cells per spleen (x10^5)
p = 0.009
Sham Stroke
F
CD11b+ CD45+ cells in aorta (x10^4)
p = 0.029
Ctrl Splenect.
G
% Plaque area per total aortic valve area
Control
Splenect.
Aortic valve level
Area under curve
0.017
Ctrl Splenect.
H
CD11b+ CD45+ cells in BM (x10^6)
I
Cells per spleen (x10^6)
J
MHCII+ monocytes (% CD11b) in spleen
Sham
Control
sRAGE
SR59230A
sRAGE + SR59230A
K
CD11b+ CD45+ cells in aorta (x10^4)
MHCII+ monocytes (% CD11b) in aorta
L
Area under curve
Sham
Control
sRAGE
SR59230A
sRAGE + SR59230A

Supplementary Materials and Methods

Transient ischemia-reperfusion stroke model. Mice were anaesthetized with isoflurane delivered in a mixture of 30% O_2 and 70% N_2O. An incision was made between the ear and the eye in order to expose the temporal bone. A laser doppler probe was affixed to the skull above the middle cerebral artery (MCA) territory, and the mice were placed in supine position. A midline neck incision was made and the common carotid artery and left external carotid artery were isolated and ligated; a 2-mm silicon-coated filament (Doccol) was introduced via a small incision in the common carotid artery and inserted into the internal carotid artery, finally occluding the MCA which was confirmed by a corresponding decrease in blood flow (decrease in the laser doppler flow signal <20% of baseline value). After 60 minutes of occlusion, the animals were re-anesthetized, and the filament was removed. After recovery, the mice were kept in their home cage with facilitated access to water and food. Sham-operated mice received the same surgical procedure, except the filament was inserted and immediately removed, after 60 minutes mice were re-anesthetized. Body temperature was maintained at 37°C throughout surgery using a feedback-controlled heating pad. The overall mortality rate in this group (excluding the Sham-operated animals) was approximately 20 %. Exclusion criteria: 1. Insufficient MCA occlusion (a reduction in blood flow to >20% of the baseline value). 2. Death during the surgery. 3. Lack of brain ischemia as quantified post-mortem by histological analysis. A stroke assessment score was acquired 1 hour after reperfusion. For scoring the animal after surgical procedure a score from 0 (no stroke) to 5 (very severe stroke) based on general activity and body asymmetry was used ("modified Bederson Score")(*1*).

Splenectomy. Mice were anaesthetized with isoflurane delivered in a mixture of 30% O_2 and 70% N_2O. A dorsal incision was made lateral to the spine and the abdominal cavity was entered. Blood vessels were ligated and spleen was removed by transecting the vessels distal to the ligature. Body temperature was maintained at 37°C throughout surgery using a

feedback-controlled heating pad. Mice were kept under controlled conditions until they were fully recovered from anesthesia.

Soluble mouse RAGE production. Soluble RAGE recombinant baculovirus was a kind gift from Dr. Ann-Marie Schmidt (New York University Langone Medical Center, USA). sRAGE recombinant virus was propagated in Sf21-cells and supernatant was kept at 4°C for further analysis and protein production. Low passage viral titer was determined by quantitative PCR (*2*). For protein production, Sf21 cells were seeded one day prior to infection with 1x106 cells/mL. Cells were infected and incubated at 27°C. Three days later, supernatant (SN) was harvest, filtered and buffer exchanged to 0.1 PBS pH 6.9/50mM NaCl. sRAGE was captured by ion-exchange chromatography using a CaptoS-5mL prepacked column (GE Healthcare) and eluted with 0.1xPBS, pH 6.9/600mM NaCl. Positive fractions were pooled, diluted 15-fold in 0.1PBS pH6.9/50mM NaCl and purified by ion-exchange chromatography using a ResourceS-1mL prepacked column (GE Healthcare). Positive fractions were pooled, dialyzed against PBS, pH 7.2, 10% glycerol at 4°C and stored at -80°C.

Drug & dye administration.

sRAGE: Mice received intraperitoneally three injections of sRAGE (Helmholtz), 30 min before, 24 h and 2 weeks after surgery. sRAGE was injected i.p. at a dose of 3.5 mg kg^{-1} body weight in a final volume of 100 µl.

HMGB1: Mice received one bolus (100µg) of either anti-HMGB1 or isotype control IgG immediately after ischemia induction. The anti-HMGB1 antibody (m2G7, IgG2b) does not recognize HMGB2 and binds to the amino acids 53-63 within the box A domain of rodent and human HMGB1 (*3*) and was purified from hybridoma supernatant by protein G affinity chromatography. The absence of endotoxin contamination was verified by Limulus assay. Recombinant HMGB1 (rHMGB1) in fully-reduced and disulfide redox-state (HMGBiotech) was injected intraperitoneally (one bolus: 5 µg of each redox form (in total 10 µg) in a final volume of 100 µl PBS).

Bromodeoxyuridine (BrdU): BrdU (BD Pharmingen) was administered using osmotic mini-pumps implanted subcutaneously (Alzet model 1002) at a dose of 50µg/d for one week. Osmotic pumps were implanted immediately after stroke or sham surgery.

Qtracker 655: Qtracker 655 (Life technologies) was injected with a 10 µl microsyringe (Hamilton) directly into the femoral bone marrow at the corpus femoris 2 h before stroke or sham surgery at a total volume of 2 µl. Administration of sterile PBS was used as a control.

Adoptive myeloid cell transfer. Donor animals (CCR2 $^{RFP/+}$ or CCR2 $^{RFP/RFP}$) were sacrificed and hind limbs were collected in Dulbecco's Modified Eagle Medium (DMEM). The muscle tissue was removed with 70 % ethanol in a petri dish. The bone marrow was flushed out of femur and tibia with DMEM using a syringe and the cell suspension was filtered through 40 µm cell strainers. After cells were washed and counted they were intraperitoneally injected in *ApoE*$^{-/-}$ recipient mice (10^7 cells per mouse) in a total volume of 200µl in saline.

Molecular MRI imaging with VCAM-1-targeted micron-sized iron oxide particles (MPIOs). MRI Experiments were carried out on a Pharmascan 7 T/12 cm system using surface coils (Bruker, Germany). Before imaging, the mice received an intravenous injection of 1 mg/kg of VCAM-1 targeted MPIOs through a tail vein catheter, as previously described (*4*). Thirty minutes thereafter, 3D T2*-weighted gradient echo imaging with flow compensation (GEFC, spatial resolution of 93µm x 70µm x 70µm interpolated to an isotropic resolution of 70 µm) using respiratory and cardiac gating (images were acquired during the end diastole), with TE/TR 6.2ms/~200ms and a flip angle (FA) of 20° was performed to visualize MPIOs bound to the aortic valve (acquisition time=8-15 min). During MRI, the mice were maintained under anesthesia with 2% isoflurane in 100% O2. For image analysis, the first step was to crop the initial MRI in a 70x70 pixels picture, including the aortic valve and the surrounding blood. Then, 3D Otsu automated threshold was applied using ImageJ software and the signal void volume was computed in mm3.

Organ and tissue processing. Mice were deeply anaesthetized with ketamine (120 mg/kg) and xylazine (16 mg/kg) and venous blood was drawn via cardiac puncture of the right ventricle in 50mM EDTA (Sigma-Aldrich); the plasma was isolated by centrifugation at 3000 relative centrifugal force (rcf) for 10min and stored at -80 °C until further use. The blood pellet was resuspended in DMEM and erythrocytes were lysed using isotonic ammonium chloride buffer. Mice were then transcardially perfused with normal saline and aorta, heart, femurs and spleen were dissected. Spleen and femurs were transferred to Hank's balanced salt solution, homogenized and filtered through 40 µm cell strainers. Erythrocytes in spleens were lysed using isotonic ammonium chloride buffer.

To isolate mononuclear cells from aorta, the whole aorta was minced into small pieces and incubated in Roswell Park Memorial Institute (RPMI) medium containing 125 U/ml collagenase XI, 60 U/ml hyaluronidase I, 60 U/ml DNase I and 450 U/ml collagenase I (Sigma Aldrich) for 30min at 37 °C (*5*). The cell suspensions were then mechanically homogenized, filtered and washed prior to flow cytometry.

Infarct volumetry. Mice were sacrificed by over dose of ketamine-xylazine and perfused intracardially with 10 mL saline solution. Brains were removed and immediately frozen in powdered dry ice. Afterwards, brains were fixed in optimum cutting temperature compound (O.C.T., Tissue-tek) solution and 20µm coronal sections were cut on every 400µm. Sections were stained with cresyl violet and scanned at 600 dpi. Infarct area on each section was analyzed by ImageJ software (NIH). The Swanson method was applied to indirectly measure the infarct area and to correct for cortical swelling: [ischemic area] = [area of the contralateral hemisphere] - [nonischemic area of the ipsilateral hemisphere]. The total infarct volume was determined by integrating measured areas and distances between sections.

Monocyte activation assay. Splenic monocytes were isolated using $CD11b^+$ magnetic-activated cell sorting (CD11b Micro beads, Miltenyi) and cultured (DMEM, 10 % FCS, 1 % Penicilin/Streptavidin) in 12-well flat-bottom plates ($5x10^5$ cells per well). Purity of monocyte

Magnetic-activated cell sorting isolation was verified by flow cytometric analysis to be ≥ 95 %. Treatment with rHMGB1 (0.1 and 0.5 μg/ml), murine stroke or sham plasma (50 % in DMEM) was given in each well individually and 4 h later cells were harvested and prepared for further analysis.

In vitro murine aortic endothelium stimulation assay. Murine aortic endothelial cells (Innoprot, Ref: P10427) were seeded in fibronectin-coated 12-well flat-bottom plates ($5x10^5$ cells per well, Basal medium, 5 % FCS and 1 % Penicillin/Streptavidin, 1 % endothelial cell growth supplement) overnight. Cells were starved for 4 h (basal medium, 1 % Penicillin/Streptavidin) and before they received treatment (recombinant TNF-α: 20 ng/ml, plasma: 50 % in DMEM, recombinant HMGB1: 0.5 μg/ml). The plasma used to stimulate MAECs was collected from stroke- or sham-operated mice 4 h post-lesion. After a 4 h stimulation interval, cells were trypsinized, harvested, washed in PBS and stored at -20°C until further analysis.

Flow cytometry analysis. The following anti-mouse antibodies were used for cell stainings: anti-CD3 (clone: 17A2, eBioscience), anti-CD4 (clone: RM4-5, eBioscience), anti-CD45 (clone: 30-F11, eBioscience), anti-CD11b (clone: M1/70, eBioscience), anti-CD11c (clone: HL3, eBioscience), anti-Ly6C (clone: HK1.4, eBioscience), anti-Ly6G (clone: RB6-8C5, eBioscience), anti-MHC class II (clone: NIMR-4, eBioscience), anti-CCR2 (clone: FAB5538A, R&D systems), BrdU (clone: MOPC-21, BD Biosciences). Stainings were performed according to the manufacturer's protocols. Flow cytometric data was aquired on a BD FACSverse flow cytometer (BD Biosciences) and analyzed using FlowJo software (Treestar).

Oil Red O lipid staining. For whole aorta en face stainings, aortas were carefully dissected and adventitial fat was thoroughly trimmed away. Aortas then were cut open, unfolded, and pinned out on a silicon-elastomer for fixation in 4% paraformaldehyde (PFA) at 4 °C overnight. The aortas then were washed for 4 h in PBS, afterwards placed in 100 % propylene

glycol for 2 min at 25 °C and finally transferred to 0.5 % Oil Red O for 3 h at 25 °C. Then aortas were washed in 85 % propylene glycol and stored in PBS until image acquisition (*6*). For lipid stainings of aortic valve sections, the ventricles were removed horizontally from dissected hearts, embedded in O.C.T compound (Tissue Tek) and consecutively cryosectioned. Sections were dried, post-fixed in 4 % PFA and stained after dehydration for 1 h in 0.5 % Oil Red O solution at 37 °C. Finally, sections were counterstained for nuclei with Mayer's Hematoxylin, air dried and mounted with pre-warmed gelatin (*6*). For lipid staining of the common carotid artery branches, the carotid bifurcation area was dissected and embedded in OCT. compound. After consecutive sectioning, lipid depositions were stained with the same Oil Red O staining protocol as stated above.

Quantification of cap thickness and plaque rupture. Aortic valve sections stained with Oil Red O and Hematoxylin were microphotographed and cap thickness was assessed. Three to five measurements representing the thinnest part of the cap were averaged for each plaque (*7*). Acute plaque rupture was accepted when a visible defect in the cap was accompanied by intrusion of erythrocytes in the plaque. In some animals, 1 or more buried fibrous caps were seen within the body of plaque which were also counted as a plaque rupture (*8*).

MMP 2 and 9 *in situ* zymography of aortic valve sections. DQ-gelatin (D12054, Invitrogen) was dissolved in reaction buffer (50 mM Tris-HCl, 150 mM NaCl, 5 mM CaCl2, 200 mM sodium azide, pH 7.6). Cryosections were incubated for 3 h at 37 °C with the gelatin-containing reaction buffer. Negative control sections were pre-incubated for 1 h with the MMP-inhibitor 1,10-Phenathroline (Sigma). Nuclei were stained with DAPI. MMP activity was detected on an Axio Observer Z1 microscope with 10x magnification and a Fluorescein isothiocyanate (FITC) filter (Carl Zeiss). Data were expressed as MMP+ area(μm^2) and normalized MMP intensity (Normalized MMP intensity = Integrated Density – (Selected valve Area x Background mean fluorescence).

Tyrosine hydroxylase (TH) stainings. Dissected femurs (see above) were decalcified in 0,4 M ethylenediaminetetraacetic acid (EDTA, pH 7.4) for 72 hours. Femurs then were embedded in OCT compound (Tissue Tek) and consecutively sectioned. Sections were blocked with 10 % goat serum and 1 % bovine serum albumin (BSA) for 2 h. After washing with 0,025 % Triton X-100 in TBS, sections were incubated with an antibody against TH (rabbit, abcam) overnight at 4 °C. After washing, sections were then incubated with secondary antibody against rabbit (alexa-647, goat, DAKO) for 90 min at room temperature. Nuclei were stained with DAPI. Pictures were acquired with a confocal microscope at 40x magnification (LSM 880 Carl Zeiss).

Enzyme linked immunosorbent assay. HMGB1 levels were measured from diluted plasma samples (1:10) using a commercial assay kit according to the manufacturer's instructions (IBL international, Hamburg). For CCL-2 levels diluted samples (1:10) were measured using an ELISA kit according to a standard protocol (eBioscience).

Quantitative real time PCR (RT-PCR). Total RNA was purified from aorta, spleen, murine aortic endothelial cells (MAECs) and isolated monocytes using a RNeasy Mini Kit (Qiagen). Equal amount of RNA from each sample was used for cDNA synthesis using High Capacity cDNA Reverse Transcription Kit (Applied Biosystems). The quantitative expression of different cytokines was measured by quantitative real-time PCR with the LightCycler 480 II (Roche) and RT^2 qPCR Primer Assays and SYBR Green ROX qPCR Mastermix (Qiagen).

Primer sequences:

IL-1β: forward ‘5-ACAGATGAAGTGCTCCTTCCA-3’, reverse ‘5-GTCGGAGATTCGTAGCTGGAT-3’

IL-6: forward ‘5-CAGTTGCCTTCTTGGGACTGA-3’, reverse ‘5-GGGAGTGGTATCCTCTGTGAAGTCT-3’

TNF-α: forward 5'-CAT CTT CTC AAA ATT CGA GTG ACA A-3', reverse5'-TGG GAG TAG ACA AGG TAC AAC CC-3'

IFN-γ: forward 5'-TGGCATAGATGTGGAAGAAAAGAG-3', reverse 5'-TGCAGGATTTTCATGTCACCAT-3'

ICAM-1: forward 5′-CAATTTCTCATGCCGCACAG-3′, reverse 5′-AGCTGGAAGATCGAAAGTCCG-3′

VCAM-1: forward 5′-TGAACCCAAACAGAGGCAGAGT-3′, reverse 5′-GGTATCCCATCACTTGAGCAGG-3'

RAGE: forward 5′-GGACCCTTAGCTGGCACTTAGA-3′, reverse5′-GAGTCCCGTCTCAGGGTGTCT-3′

PPIA: forward '5-ACGCCACTGTCGCTTTTC-3', reverse '5-ACCCGACCTCGAAGGAGA-3'

GAPDH: forward 5'-TGACGTGCCGCCTGGAGAAA-3', reverse 5'-AGTGTAGCCCAAGATGCCCTTCAG-3'

RT-PCR array. The RT^2 PreAMP cDNA syntesis Kit (Qiagen) was used for the cDNA synthesis and RT^2 Profiler PCR Array for chemokines and chemokine receptors (PAMM-022Z, Qiagen) was measured in a Roche LightCycler 480. Finally, data was analyzed with RT^2 Profiler PCR Array Data analysis software (version3.5) from SABiosciences.

Quantification of patient infarct volumes. Infarct volumes were quantified on images from diagnostic scans, either computed tomography or magnetic resonance imaging (diffusion-weighted, T2 or fluid-attenuated inversion recovery). The modality and image with the largest infarct size was used for volumetry. Trained raters segmented infarcts manually slice-by-slice. The inter-rater reliability for this procedure showed an intraclass correlation coefficient of 0.993.

Analysis of HMGB1 isoforms by electrospray ionization liquid chromatography tandem mass spectrometry (ESI-LC-MS/MS). Samples were pre-cleared with 50 µl protein G-Sepharose beads for 1h at 4°C and HMGB1 present was immunoprecipitated with 5 µg of rabbit anti-HMGB1 (ab18256) for 16 h at 4°C as previously described (9). For the analysis of

HMGB1 post translational modifications, free thiol groups within HMGB1 were alkylated for 90 min with 10 mM iodoacetamide at 4°C. Cysteine residues in disulfide bonds were then reduced with 30 mM dithiothreitol at 4°C for 1 h followed by alkylation of newly exposed thiol groups with 90 mM NEM at 4°C for 10 min as previously described (*10, 11*). Samples were subjected to trypsin (Promega) or GluC (New England Biolabs) digestion according to manufacturer's instructions and de-salted using C18 zip-tips (Millipore). Characterization of post translational modifications within HMGB1 were determined as described previously using an AB Sciex QTRAP 5500 (Sciex Inc.) equipped with a NanoSpray II source by in-line liquid chromatography using a U3000 HPLC System (Dionex), connected to a 180 µm x 20 mm nanoAcquity UPLC C18 trap column and a 75 µm x 15 cm nanoAcquity UPLC BEH130 C18 column (Waters) via reducing unions. A gradient from 0.05% TFA (v/v) to 50% ACN/0.08% TFA (v/v) in 40 min was applied at a flow rate of 200 nL/min (*12*). The ion spray potential was set to 2,200-3,500 V, the nebulizer gas to 19 L/min and the interface heater to 150°C. Accurate mass and whole protein electrospray ionisation (ESI) mass spectrometry is determine as previously described using a AB Sciex TripleToF 5600+ system (*12*).

References

1. J. B. Bederson, L. H. Pitts, M. Tsuji, M. C. Nishimura, R. L. Davis, H. Bartkowski, Rat middle cerebral artery occlusion: evaluation of the model and development of a neurologic examination. *Stroke* **17**, 472-476 (1986).
2. H. R. Lo, Y. C. Chao, Rapid titer determination of baculovirus by quantitative real-time polymerase chain reaction. *Biotechnol Prog* **20**, 354-360 (2004).
3. S. Qin, H. Wang, R. Yuan, H. Li, M. Ochani, K. Ochani, M. Rosas-Ballina, C. J. Czura, J. M. Huston, E. Miller, X. Lin, B. Sherry, A. Kumar, G. Larosa, W. Newman, K. J. Tracey, H. Yang, Role of HMGB1 in apoptosis-mediated sepsis lethality. *J Exp Med* **203**, 1637-1642 (2006).
4. M. Gauberti, A. Montagne, O. A. Marcos-Contreras, A. Le Behot, E. Maubert, D. Vivien, Ultra-sensitive molecular MRI of vascular cell adhesion molecule-1 reveals a dynamic inflammatory penumbra after strokes. *Stroke* **44**, 1988-1996 (2013).
5. M. J. Butcher, M. Herre, K. Ley, E. Galkina, Flow cytometry analysis of immune cells within murine aortas. *Journal of visualized experiments : JoVE*, (2011).
6. E. Maganto-Garcia, M. Tarrio, A. H. Lichtman, Mouse models of atherosclerosis. *Current protocols in immunology* **Chapter 15**, Unit 15 24 11-23 (2012).
7. T. A. Seimon, Y. Wang, S. Han, T. Senokuchi, D. M. Schrijvers, G. Kuriakose, A. R. Tall, I. A. Tabas, Macrophage deficiency of p38alpha MAPK promotes apoptosis and plaque necrosis in advanced atherosclerotic lesions in mice. *The Journal of clinical investigation* **119**, 886-898 (2009).

8. J. Johnson, K. Carson, H. Williams, S. Karanam, A. Newby, G. Angelini, S. George, C. Jackson, Plaque rupture after short periods of fat feeding in the apolipoprotein E-knockout mouse: model characterization and effects of pravastatin treatment. *Circulation* **111**, 1422-1430 (2005).
9. D. J. Antoine, D. P. Williams, A. Kipar, R. E. Jenkins, S. L. Regan, J. G. Sathish, N. R. Kitteringham, B. K. Park, High-mobility group box-1 protein and keratin-18, circulating serum proteins informative of acetaminophen-induced necrosis and apoptosis in vivo. *Toxicological sciences : an official journal of the Society of Toxicology* **112**, 521-531 (2009).
10. S. Nystrom, D. J. Antoine, P. Lundback, J. G. Lock, A. F. Nita, K. Hogstrand, A. Grandien, H. Erlandsson-Harris, U. Andersson, S. E. Applequist, TLR activation regulates damage-associated molecular pattern isoforms released during pyroptosis. *EMBO J* **32**, 86-99 (2013).
11. E. Venereau, M. Casalgrandi, M. Schiraldi, D. J. Antoine, A. Cattaneo, F. De Marchis, J. Liu, A. Antonelli, A. Preti, L. Raeli, S. S. Shams, H. Yang, L. Varani, U. Andersson, K. J. Tracey, A. Bachi, M. Uguccioni, M. E. Bianchi, Mutually exclusive redox forms of HMGB1 promote cell recruitment or proinflammatory cytokine release. *The Journal of experimental medicine* **209**, 1519-1528 (2012).
12. X. Ge, D. J. Antoine, Y. Lu, E. Arriazu, T. M. Leung, A. L. Klepper, A. D. Branch, M. I. Fiel, N. Nieto, High mobility group box-1 (HMGB1) participates in the pathogenesis of alcoholic liver disease (ALD). *J Biol Chem* **289**, 22672-22691 (2014).

Supplementary Figures

Figure S1

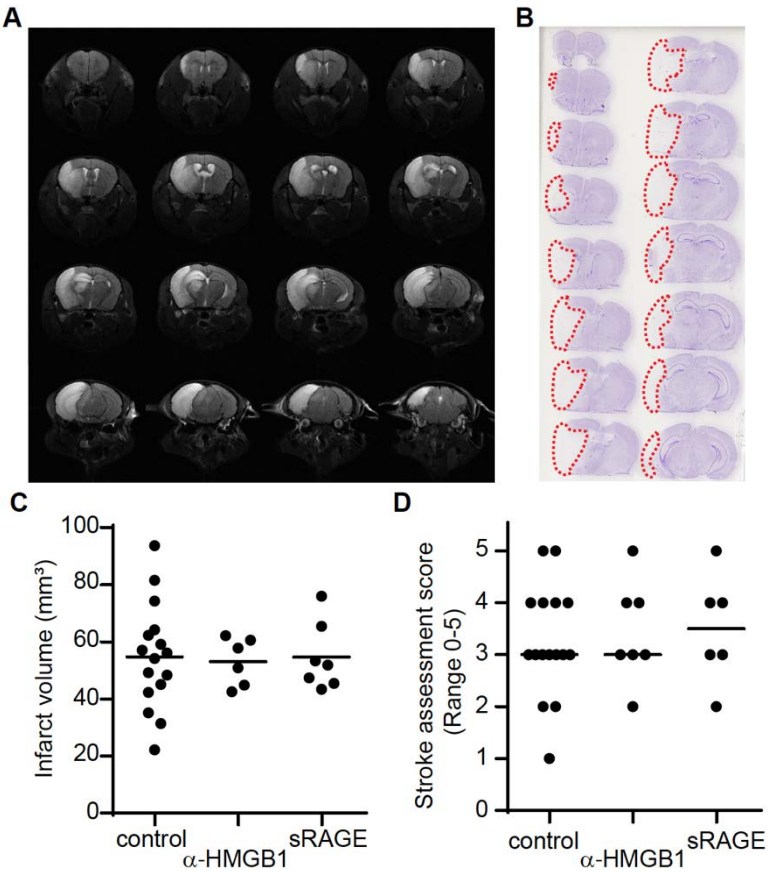

Figure S1. Characterization of the 60 minutes filament MCA occlusion (fMCAo) model. (**A**) Coronal brain sections from T2w MRI of an in infarcted brain 5 days after 60 min fMCAo surgery. (**B**) Cresyl violet histology of coronal sections of an infarcted brain 7 days after fMCAo. (**C**) Quantification of brain infarct volume cresyl violet histology of a untreated compared to anti-HMGB1 antibody and sRAGE treated brains. (**D**) Comparison of stroke assessment scores 1 h after reperfusion in fMCAo mice (n= 6-16 per group). All mice used are HCD-fed ApoE$^{-/-}$ mice.

Figure S2

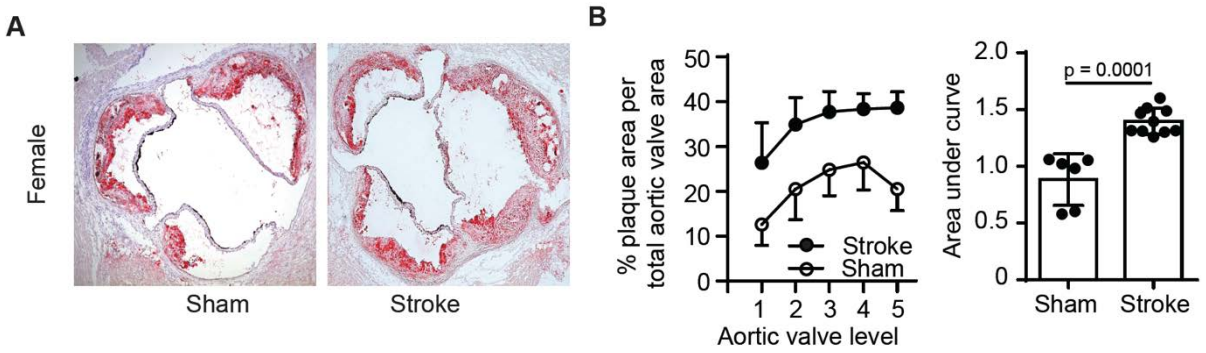

Figure S2. Atherosclerotic lesions in aortic valves of male and female HCD-fed ApoE$^{-/-}$ mice one month after fMCAo surgery. (**A**) Representative images of Oil Red O aortic valve quantification of female HCD-fed ApoE$^{-/-}$ mice one month after stroke or sham surgery. (**B**) Plaque area quantification of 5 consecutive levels in aortic valves (left) and area under curve (AUC, right) analysis in stroke and sham-operated mice one month after surgery (U Test, 8-10 per group). All data in panel B are shown as mean with error bars indicating s.d.

Figure S3

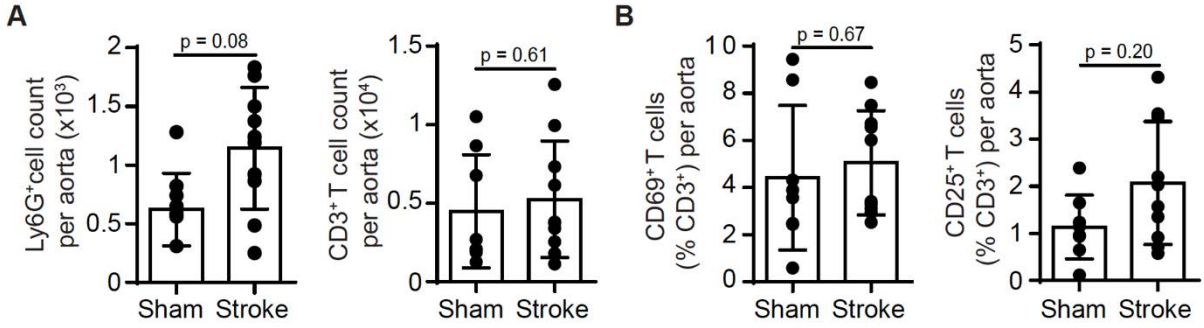

Figure S3. Immune cell count in aorta of HCD-fed ApoE$^{-/-}$ mice one month after experimental stroke. (**A**) CD45^{+}Ly6G^{+} granulocytes (left) and CD45^{+}CD3^{+} T cells (right) cell counts after sham or stroke surgery. (**B**) Percentage of CD69^{+} (left) and CD25^{+} (right) T cell subsets after sham or stroke surgery. (U Test, n= 8-10 per group).

Figure S4

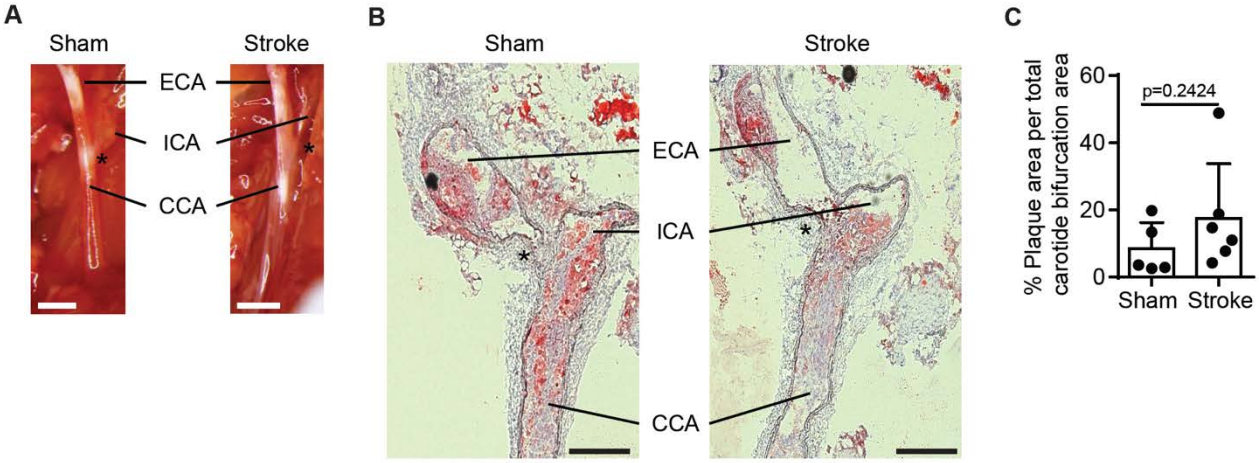

Figure S4. Analysis of atherosclerotic plaque load at the common carotid artery bifurcation in HCD-fed ApoE$^{-/-}$ mice. (**A**) Representative microphotographs of the common carotid artery bifurcation on the contralateral side 7 days after stroke or sham surgery (scale bar = 1mm, * indicates bifurcation). (**B**) Representative Oil Red O stained longitudinal common carotid artery bifurcation sections (scale bar = 500µm, * indicates bifurcation). (**C**) Quantification of Oil Red O+ plaque load in the contralateral common carotid artery lumen 7 days after stroke or sham surgery (U Test, n= 5-6 per group). CCA = common carotid artery, ICA = internal carotid artery, ECA = external carotid artery.

Figure S5

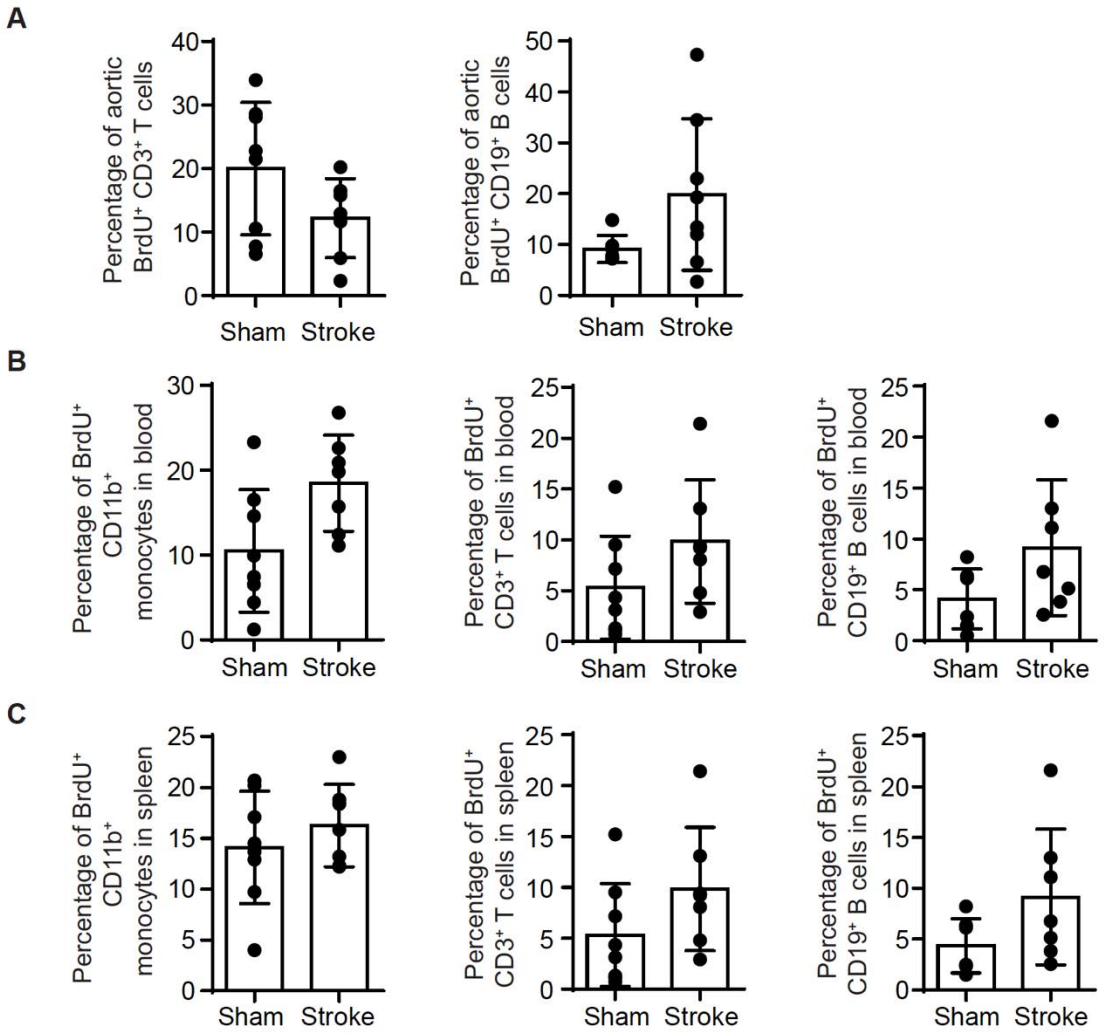

Figure S5. Comparison of Bromdesoxyuridine (BrdU) incorporation in aorta, blood and spleen one week after experimental stroke surgery. (A) Percentage of $BrdU^+$ $CD3^+$ T cells (left) and $BrdU^+$ $CD19^+$ B cells in aorta after stroke or sham surgery. (B, C) Percentage of $BrdU^+$ cells in blood (**B**) and spleen (**C**) after experimental stroke or sham surgery (U Test, n= 6-8 mice per group). All bar graphs are shown as mean ± s.d.

Figure S6

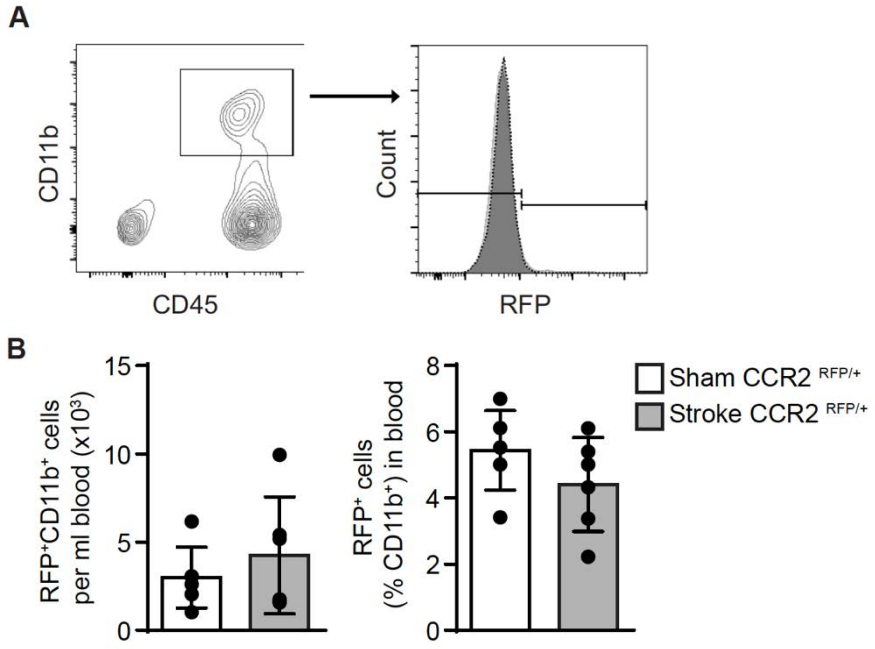

Figure S6. RFP$^+$CD11b$^+$ cell counts in blood one week after experimental stroke surgery. HCD-fed ApoE$^{-/-}$ mice underwent sham or stroke surgery received CCR2RFP/+ bone marrow cell (BMC) transplantation (10^7 cells) immediately after surgery. One week later mice were sacrificed and blood analyzed. (**A**) Flow cytometric gating strategy to analyze RFP$^+$CD11b$^+$ cells in blood. (**B**) Quantification of total RFP$^+$CD11b$^+$ cell counts in blood one week after sham or stroke surgery (left). Percentage of RFP$^+$CD11b$^+$ cells in blood one week after sham or stroke surgery (right, U Test, n= 5-6 mice per group). All bar graphs are shown as mean ± s.d.

Figure S7

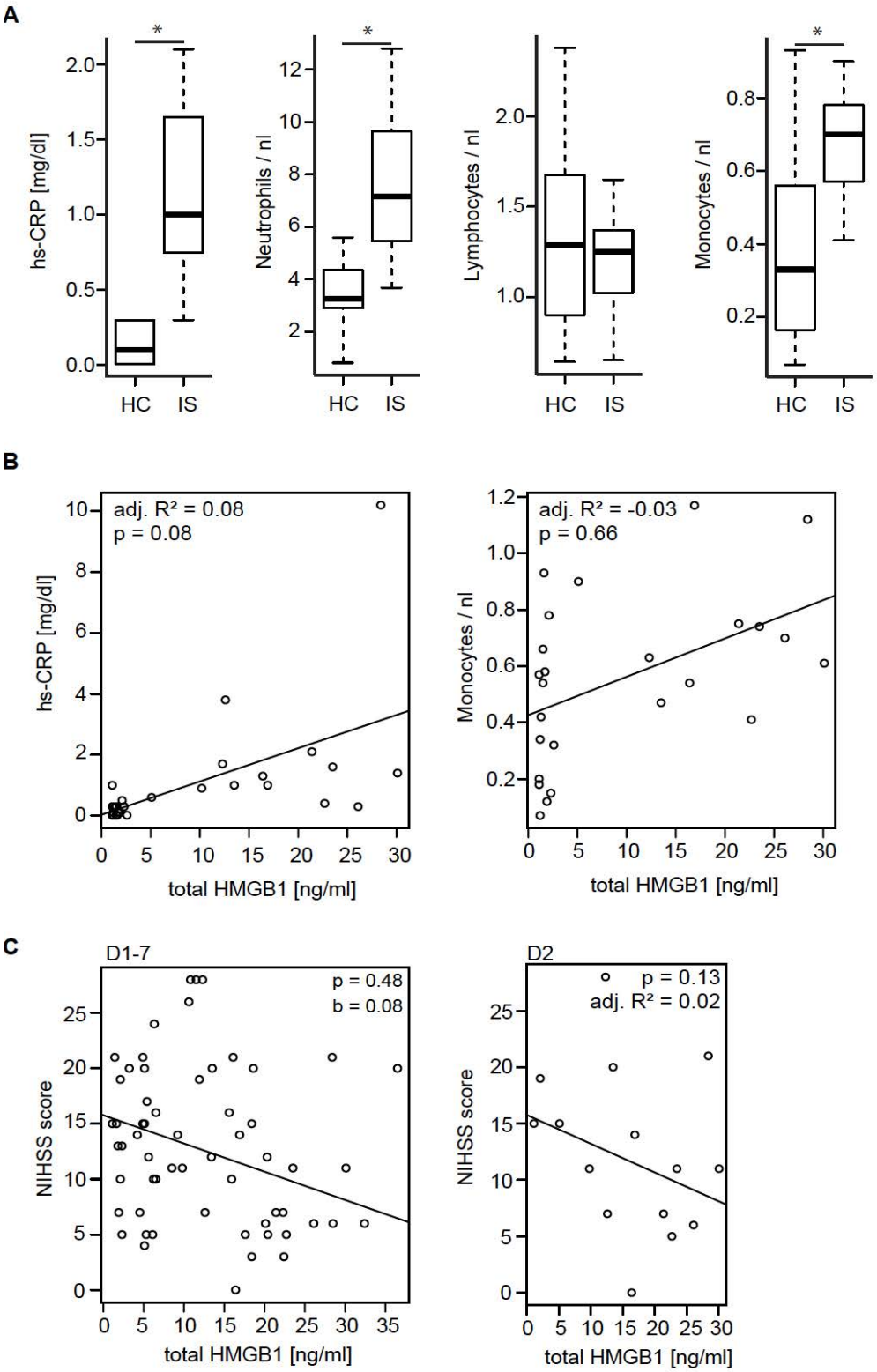

Figure S7. Immunological data of stroke patients. (**A**) Comparison of hs-CRP and leukocyte subpopulations between HCs and patients with IS at day 2 (Wilcoxon rank sum test) (**B**) Regression of total HMGB1 levels with hs-CRP or monocytes/nl of HCs and IS patients at day 2 after stroke (Linear regression analysis with adjustment for groups). (**C**) Regression analysis of NIHSS scores and total HMGB1 levels in patients with IS from admission to day 7 after stroke (Linear mixed model with day as random effect). Abbreviations: NIHSS, National Institute of Health stroke scale; IS, ischemic stroke.

Figure S8

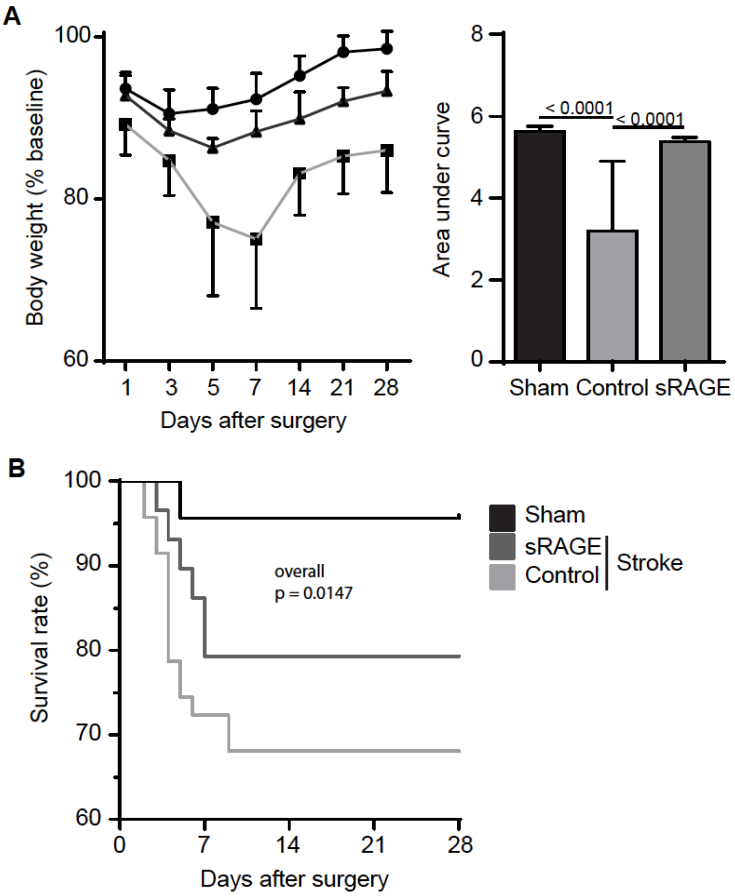

Figure S8. Body weight and mortality in sRAGE treatment mice after stroke. (**A**) Body weight curves (left, indicated as % body weight to individual baseline before stroke) after sham and stroke surgery with vehicle or sRAGE treatment. Area under curve analysis (right) for statistical analysis of indicated groups (U Test, n= 10-15 mice per group, graphs shown as mean ± s.d.). (**B**) Kaplan-Meier curves of post-stroke survival within one month after stroke in vehicle or sRAGE treated and sham-operated mice (Comparison of differences between curves by Mantel-Cox Test , n= 28-47).

Figure S9

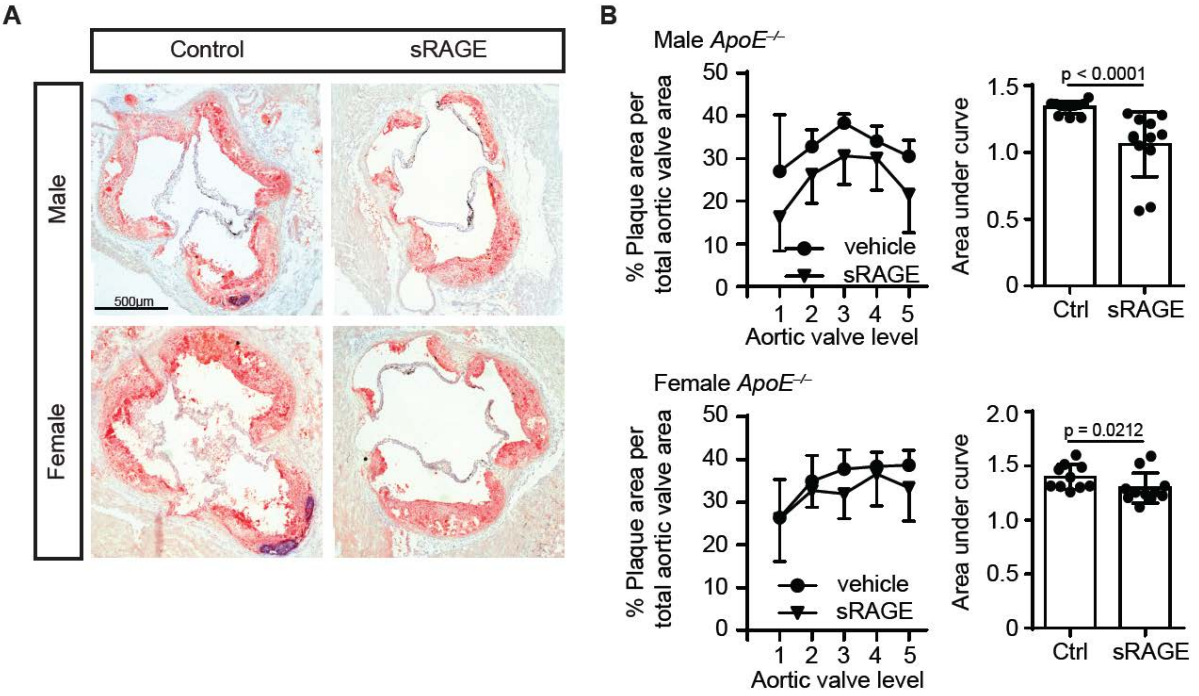

Figure S9. Atherosclerotic lesions in aortic valves of male and female HCD-fed ApoE$^{-/-}$ mice one month after experimental stroke and sRAGE treatment. (**A**) Representative images of Oil Red O aortic valve sections of male and female HCD-fed ApoE$^{-/-}$ mice with vehicle or sRAGE treatment 4 weeks after stroke surgery. (**B**) Plaque area quantification of 5 consecutive levels in aortic valves and area under curve (AUC) analysis of stroke (± sRAGE) for male and female mice (U Test, n= 8-10 mice per group). All graphs are shown as mean with error bars indicating s.d.

Figure S10

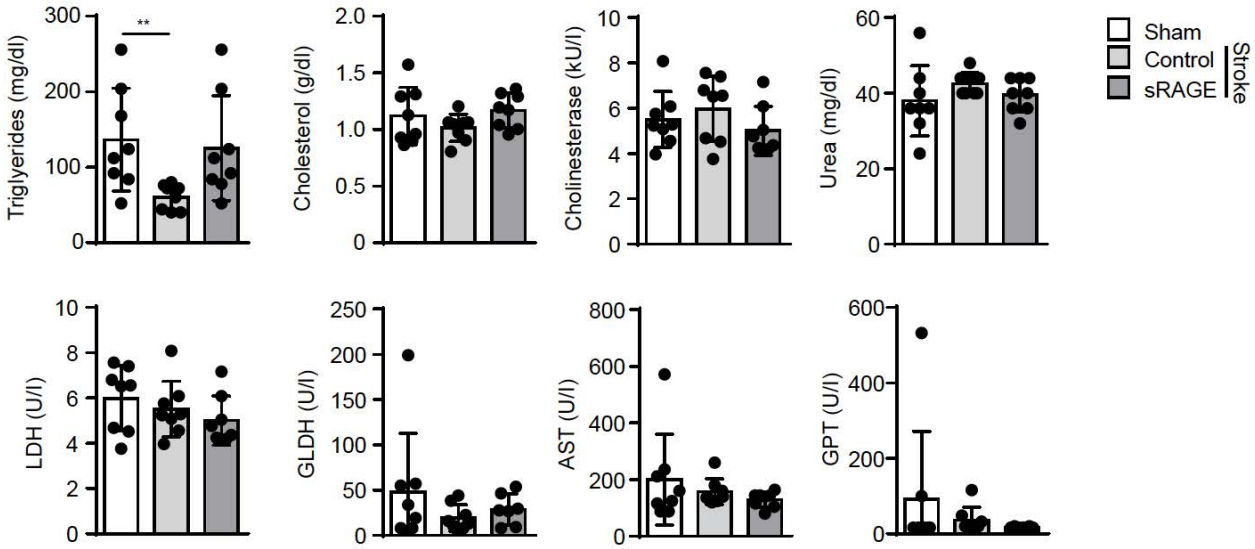

Figure S10. Lipid profile of plasma samples one month after experimental stroke surgery and sRAGE treatment. Triglycerides, cholesterol, cholinesterase, urea, lactate dehydrogenase (LDH), glutamate dehydrogenase (GLDH), aspartate aminotransferase (AST) and glutamic pyruvic transaminase (GPT) concentrations after experimental stroke or sham surgery (± sRAGE) in HCD-fed ApoE$^{-/-}$ mice. (One way-ANOVA; n= 8-9 mice per group). All bar graphs are shown as mean ± s.d.

Figure S11

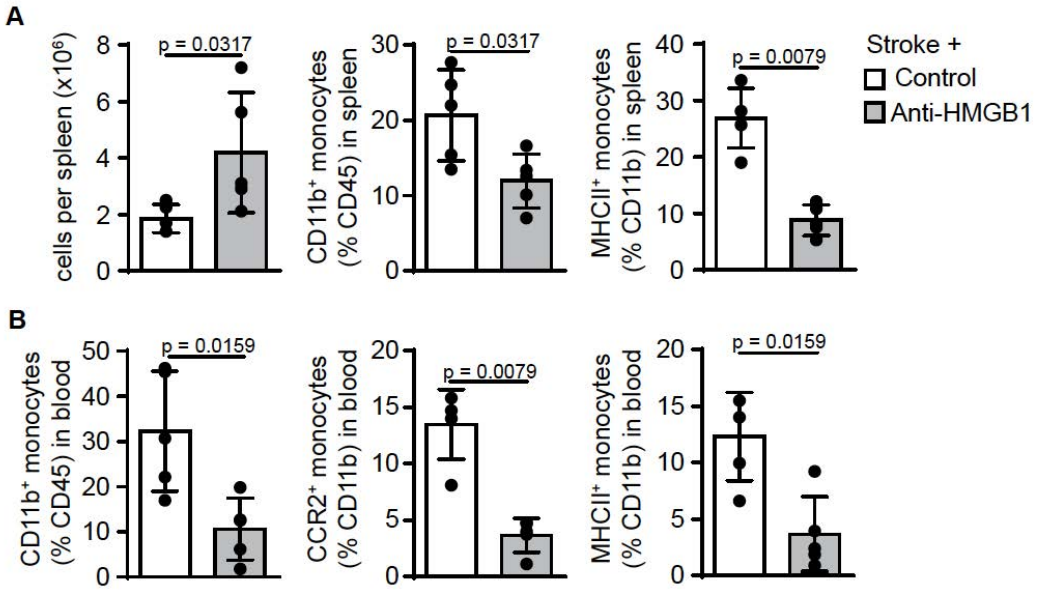

Figure S11. Flow cytometric analysis of spleen and blood 24 h after experimental stroke with anti-HMGB1 treatment. (**A**) Flow cytometric analysis of WT mice treated with IgG control or HMGB1-specific monoclonal antibodies (anti-HMGB1) 24 h after stroke surgery. Whole $CD45^+$ spleen cell counts (left) and percentages of $CD11b^+$ (middle) and $CD11b^+MHCII^+$ (right) cells were measured. (**B**) Flow cytometric analysis of $CD45^+CD11b^+$ (left), $CD11b^+CCR2^+$ (middle) and CD11b+MHCII+ (right) cell percentages from blood 24 h after stroke ± anti-HMGB1 treatment (U Test, n= 5-8 mice per group). All bar graphs are shown as mean ± s.d.

Figure S12

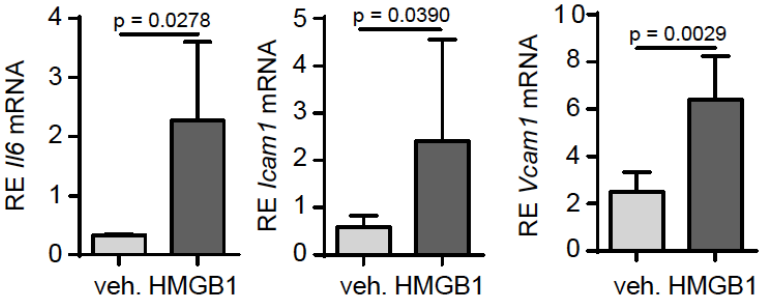

Figure S12. Recombinant HMGB1 in vivo administration exacerbates atherosclerosis. HCD-fed ApoE$^{-/-}$ mice received i.p. injection of a single bolus of 10 µg rHMGB1. After one week mice were sacrificed and aorta and aortic valve were analyzed. Expression of *Il-6* (left), *Icam-1* (middle) and *Vcam-1* (right) (RE, relative expression) was analyzed from aorta lysates (U Test, n= 5 per group). All graphs are shown as mean ± s.d.

Figure S13

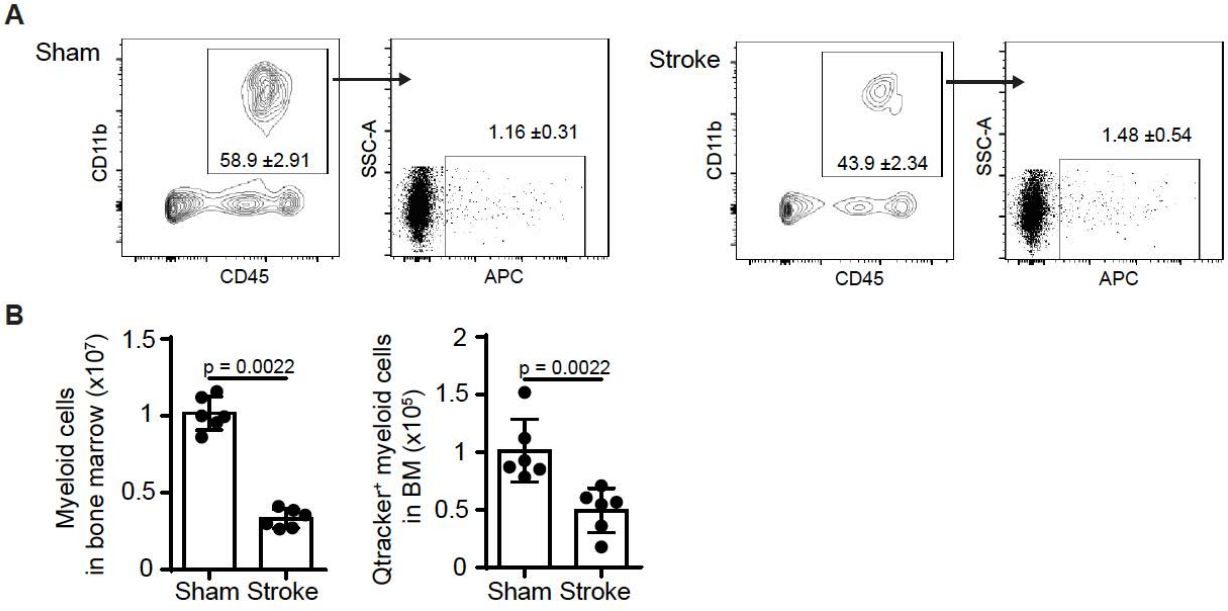

Figure S13. Quantification of in vivo Qdot labeling of femoral bone marrow 24 h after experimental stroke. WT mice received Qdot administration in the femoral bone marrow 2h before sham or stroke surgery and were sacrificed 24 h later. (**A**) Representative gating strategy for $CD45^{+}CD11b^{+}$ monocytes and Qdot+ monocytes in femoral bone marrow after stroke or sham surgery. (**B**) Quantification of myeloid cells (left) and Qdot+ monocytes (right) in femoral bone marrow (U Test, n= 6 per group). All graphs are shown as mean ± s.d.

Figure S14

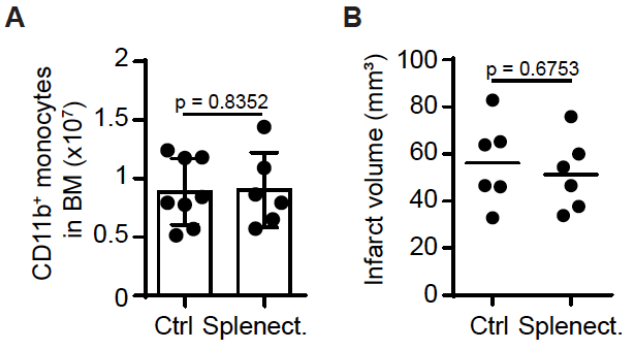

Figure S14. Myeloid cell count in femoral bone marrow and brain infarct volumetry after splenectomy. Spleen of HCD-fed ApoE$^{-/-}$ mice were removed surgically or sham surgery was performed before experimental stroke was induced. One week later mice were sacrificed and analyzed for myeloid cell counts and infarct volumetry. (**A**) Flow cytometric analysis of bone marrow from either splenectomized or sham operated mice after experimental stroke (U Test, n= 6-8 per group). (**B**) Cresyl violet histology of infarcted brains from stroked mice with either splenectomy or sham surgery (U Test, n=6 per group). All graphs shown as mean ± s.d.

Figure S15

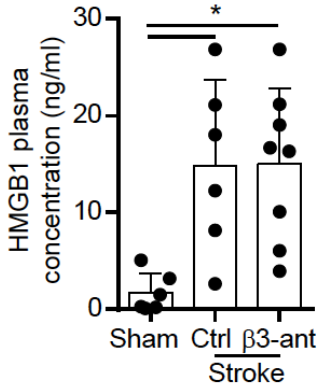

Figure S15. Impact of beta-3-adrenoreceptor blockage on HMGB1 plasma levels after experimental stroke. HMGB1 plasma concentrations were measured by ELISA in sham and stroke-operated (± SR59230A treatment) HCD-fed ApoE$^{-/-}$ mice 7d after surgery (H Test, n= 6-8 per group). Graph is shown as mean ± s.d. (* = p value <0.05).

Figure S16

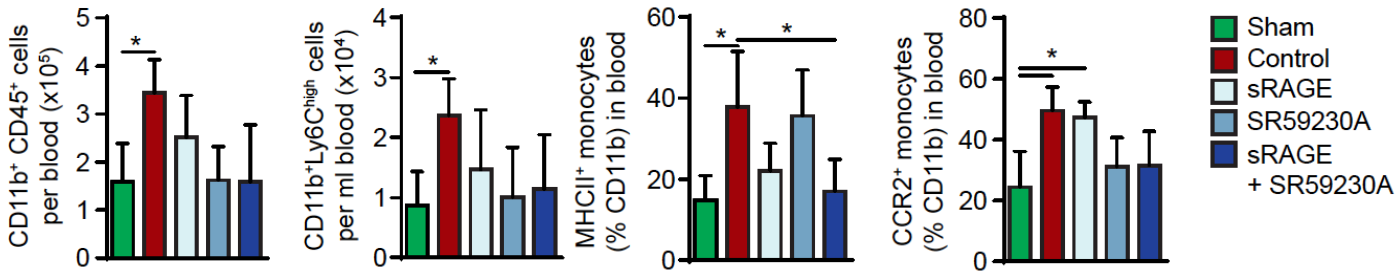

Figure S16. Impact of beta-3-adrenoreceptor blockage (SR59230A), alarmin blockage (sRAGE) and combined treatment on blood immune cells in WT mice. WT mice received either SR59230A, sRAGE, both combined or control treatment immediately after stroke and blood was analyzed by flow cytometry 24 h later for total myeloid ($CD45^+CD11b^+$), $CD11b^+Ly6C^{high}$, MHCII and CCR2 expressing cells (H Test, n= 6-8 per group). All graphs are shown as mean ± s.d. (*: $p < 0.05$)

Figure S17

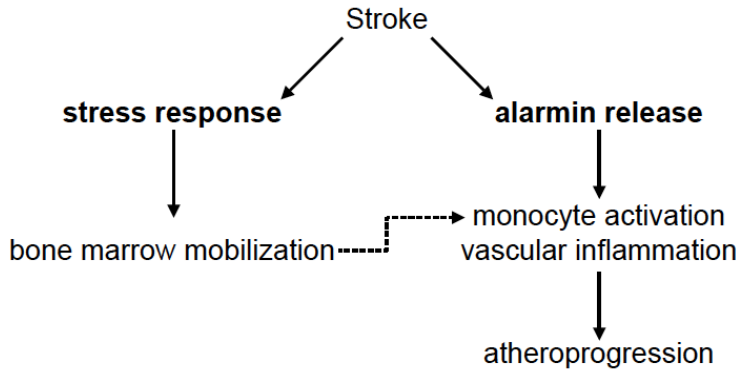

Figure S17. Schematic overview of proposed mechanism of atheroprogression after stroke.

Table S1: Primer list for qPCR array (Mouse chemokines and receptors)

Symbol	Description
C5ar1	Complement component 5a receptor 1
Ackr2	Chemokine binding protein 2
Ccl1	Chemokine (C-C motif) ligand 1
Ccl11	Chemokine (C-C motif) ligand 11
Ccl12	Chemokine (C-C motif) ligand 12
Ccl17	Chemokine (C-C motif) ligand 17
Ccl19	Chemokine (C-C motif) ligand 19
Ccl2	Chemokine (C-C motif) ligand 2
Ccl20	Chemokine (C-C motif) ligand 20
Ccl22	Chemokine (C-C motif) ligand 22
Ccl24	Chemokine (C-C motif) ligand 24
Ccl25	Chemokine (C-C motif) ligand 25
Ccl26	Chemokine (C-C motif) ligand 26
Ccl28	Chemokine (C-C motif) ligand 28
Ccl3	Chemokine (C-C motif) ligand 3
Ccl4	Chemokine (C-C motif) ligand 4
Ccl5	Chemokine (C-C motif) ligand 5
Ccl6	Chemokine (C-C motif) ligand 6
Ccl7	Chemokine (C-C motif) ligand 7
Ccl8	Chemokine (C-C motif) ligand 8
Ccl9	Chemokine (C-C motif) ligand 9
Ccr1	Chemokine (C-C motif) receptor 1
Ccr10	Chemokine (C-C motif) receptor 10
Ccr1l1	Chemokine (C-C motif) receptor 1-like 1
Ccr2	Chemokine (C-C motif) receptor 2
Ccr3	Chemokine (C-C motif) receptor 3
Ccr4	Chemokine (C-C motif) receptor 4
Ccr5	Chemokine (C-C motif) receptor 5
Ccr6	Chemokine (C-C motif) receptor 6
Ccr7	Chemokine (C-C motif) receptor 7
Ccr8	Chemokine (C-C motif) receptor 8
Ccr9	Chemokine (C-C motif) receptor 9
Ackr4	Chemokine (C-C motif) receptor-like 1
Ccrl2	Chemokine (C-C motif) receptor-like 2
Cmklr1	Chemokine-like receptor 1
Cmtm2a	CKLF-like MARVEL transmembrane domain containing 2A
Cmtm3	CKLF-like MARVEL transmembrane domain containing 3
Cmtm4	CKLF-like MARVEL transmembrane domain containing 4
Cmtm5	CKLF-like MARVEL transmembrane domain containing 5
Cmtm6	CKLF-like MARVEL transmembrane domain containing 6
Cx3cl1	Chemokine (C-X3-C motif) ligand 1
Cx3cr1	Chemokine (C-X3-C) receptor 1
Cxcl1	Chemokine (C-X-C motif) ligand 1
Cxcl10	Chemokine (C-X-C motif) ligand 10
Cxcl11	Chemokine (C-X-C motif) ligand 11
Cxcl12	Chemokine (C-X-C motif) ligand 12
Cxcl13	Chemokine (C-X-C motif) ligand 13
Cxcl14	Chemokine (C-X-C motif) ligand 14
Cxcl15	Chemokine (C-X-C motif) ligand 15
Cxcl16	Chemokine (C-X-C motif) ligand 16
Cxcl2	Chemokine (C-X-C motif) ligand 2
Cxcl3	Chemokine (C-X-C motif) ligand 3
Cxcl5	Chemokine (C-X-C motif) ligand 5
Cxcl9	Chemokine (C-X-C motif) ligand 9
Cxcr1	Chemokine (C-X-C motif) receptor 1
Cxcr2	Chemokine (C-X-C motif) receptor 2
Cxcr3	Chemokine (C-X-C motif) receptor 3

Cxcr4	Chemokine (C-X-C motif) receptor 4
Cxcr5	Chemokine (C-X-C motif) receptor 5
Cxcr6	Chemokine (C-X-C motif) receptor 6
Ackr3	Chemokine (C-X-C motif) receptor 7
Ackr1	Duffy blood group, chemokine receptor
Fpr1	Formyl peptide receptor 1
Gpr17	G protein-coupled receptor 17
Hif1a	Hypoxia inducible factor 1, alpha subunit
Ifng	Interferon gamma
Il16	Interleukin 16
Il1b	Interleukin 1 beta
Il4	Interleukin 4
Il6	Interleukin 6
Itgam	Integrin alpha M
Itgb2	Integrin beta 2
Mapk1	Mitogen-activated protein kinase 1
Mapk14	Mitogen-activated protein kinase 14
Pf4	Platelet factor 4
Ppbp	Pro-platelet basic protein
Slit2	Slit homolog 2 (Drosophila)
Tgfb1	Transforming growth factor, beta 1
Tlr2	Toll-like receptor 2
Tlr4	Toll-like receptor 4
Tnf	Tumor necrosis factor
Tymp	Thymidine phosphorylase
Xcl1	Chemokine (C motif) ligand 1
Xcr1	Chemokine (C motif) receptor 1
Actb	Actin, beta
B2m	Beta-2 microglobulin
Gapdh	Glyceraldehyde-3-phosphate dehydrogenase
Gusb	Glucuronidase, beta
Hsp90ab1	Heat shock protein 90 alpha (cytosolic), class B member 1

Table S2: Demographic and clinical characteristics of the study population

Characteristics	Stroke	Control
Demographic characteristics		
Total, n	18	12
Age, mean (SD) [years]	72.7 (14.3)	72.1 (5.9)
Female, n (%)	7 (38.9)	8 (66.7)
Vascular risk factors, n (%)		
Hypertension	15 (83.3)	4 (33.3)
Smoking history	8 (47.1)	3 (25)
Hypercholesterolemia	2 (11.8)	1 (8.3)
Obesity	4 (26.7)	1 (8.3)
Diabetes mellitus	1 (5.6)	0 (0)
Previous TIA/stroke/MI	5 (27.8)	0 (0)
ΔT, mean (SD) [hours]	5.5 (5.6)	n/a
Infarct volumes, mean (SD) [ml]	74.4 (48.0)	n/a

SD, standard deviation; TIA, transient ischemic attack; MI, myocardial infarction; ΔT, time from symptom onset until hospital arrival; n/a, not available.

Table S3: Number of (excluded/included) animals in accomplished experiments

Experiment	Total animals	Included animals	Excluded animals	Reason for exclusion
Aorta *en face* Oil Red O	20	16	4	Died after surgery
4 w Aortic valve Oil Red O & Aorta Flow cytometry	30	24	6	Died after surgery
BrdU assay	15	14	1	Died during surgery
3 d aorta lysates and CCR2 FACS	14	14	0	-
RFP^{+} transplantation	15	11	2 2	Died after surgery Transplantation failed
RFP^{het} vs. RFP^{hom}	12	11	1	Died after surgery
VCAM1 MRI	10	5	4 1	MRI scan quality Died after surgery
MAEC stimulation	35	35	-	-
HMGB1 1d ELISA	14	14	-	-
3 d sRAGE treatment	24	24	-	-
Monocyte stimulation	25	24	1	Died during surgery
4 w sRAGE treatment	12	8	4	Died after surgery
siRNA assay	28	21	4 3	Failed siRNA injection Died during procedure
Anti-HMGB1 ApoE	24	20	3 1	Died after surgery No infarct detected
Anti-HMGB1 Bl6	20	20	.	-
HMGB1 administration	15	-	-	-
Qdot tracker	14	12	2	Qdot administration failed
Splenectomy	15	14	1	Died during surgery
Beta3-blocker	40	35	3 2	Died during surgery No infarct detected

4 w, 4 weeks; 3 d, 3 days; het, heterozygous; hom, homozygous.

Table S4: Author contribution to performing and analyzing specific experiments

Experiment	Performance	Analysis
Aorta *en face* Oil Red O	SR	SR, CH
4w Aortic valve Oil Red O & Aorta Flow cytometry	SR	SR, CH, AL
BrdU assay	SR	SR, AL
3 d aorta lysates and CCR2 FACS	SR, VS	SR, VS, AL
RFP^{+} transplantation	SR	SR, AL
RFP^{het} vs RFP^{hom}	SR	SR, AL
VCAM1 MRI	SR, AA, AF	CO, MG
MAEC stimulation	SR, LS	SR, LS, AL
HMGB1 1d ELISA	SR	SR, VS
3d sRAGE treatment	SR	SR, AL
Monocyte stimulation	SR, VS	VS, AL
4w sRAGE treatment	SR	SR, AL
siRNA assay	SR	SR, AL
Anti-HMGB1 ApoE	SR	SR, AL
Anti-HMGB1 Bl6	SR	SR, AL
HMGB1 administration	SR	SR, AL
Qdot tracker	SR, VS	SR, AL, VS
Splenectomy	SR	SR, AL
Blood biochemistry	SR, LH	LH
Beta3-blocker	SR	SR, AL
Patient Cohort	ST	ST
HMGB1 MS/MS	DA	DA, SR